THE ASTROPHYSICAL JOURNAL, 413:116–136, 1993 August 10

THE *HUBBLE SPACE TELESCOPE* QUASAR ABSORPTION LINE KEY PROJECT. III. FIRST OBSERVATIONAL RESULTS ON MILKY WAY GAS[1]

BLAIR D. SAVAGE,[2] LIMIN LU,[2] JOHN N. BAHCALL,[3] JACQUELINE BERGERON,[4] ALEC BOKSENBERG,[5]
GEORGE F. HARTIG,[6] BUELL T. JANNUZI,[3] SOFIA KIRHAKOS,[3] FELIX J. LOCKMAN,[7]
W. L. W. SARGENT,[8] DONALD P. SCHNEIDER,[3] DAVID TURNSHEK,[9]
RAY J. WEYMANN,[10] AND ARTHUR M. WOLFE[11]
Received 1992 October 27; accepted 1993 February 19

ABSTRACT

We report on absorption by Milky Way disk and halo gas seen in Quasar Absorption Line Key Project measurements of 15 quasars obtained with the Faint Object Spectrograph (FOS) of the *Hubble Space Telescope* (*HST*). The measurements extend from 1150 to 3270 Å for four objects and from 1600 to 3270 Å for 11 objects and have a velocity resolution (FWHM) of 220–240 km s^{-1} and signal-to-noise ratio of typically 25 per resolution element. The data processing techniques are presented in Key Project Papers I and II. Milky Way absorption lines comprise 44% of all absorption lines found in the first group of 13 Key Project spectra. The Milky Way lines observed in the highest quality data for 3C 273 and H1821+643 include lines from H I, C II, C II*, C IV, O I, N I, Mg I, Mg II, Al II, Al III, Si II, Si III, Si IV, S II, Mn II, Fe II, and Zn II. Strong singly ionized metal lines of Fe II $\lambda\lambda$2600.17 and 2586.65 and Mg II $\lambda\lambda$2796.35 and 2803.53 are detected in all the spectra. High-quality H I 21 cm emission spectra are used to make small adjustments to the FOS wavelength scale to bring the UV data onto an LSR velocity system. The strong metal lines of Fe II and Mg II permit a sensitive search for metal-line analogs to the high-velocity clouds seen in H I 21 cm emission. Toward three quasars we detect resolved, very high negative velocity ($v < -250$ km s^{-1}) metal-line absorption. Toward four quasars we detect blended high negative velocity absorption (-250 km s$^{-1} < v < -100$ km s^{-1}). Therefore, seven of 15 sight lines observed in this limited sample exhibit high-velocity or very high velocity metal-line absorption. Lower limits to the Mg-to-H abundance ratio of 0.059, 0.12, and 0.32 times the solar abundance are obtained for the three detections of very high velocity Mg II absorption toward PKS 2251+11, PG 0043+039, and 3C 454.3, respectively. However, cloud clumping may influence this result, since the H I reference column density from 21 cm emission measurements is obtained with a 21′ beam. The sight line to PG 1259+593 reveals absorptions in the lines of Mg II, Fe II, C II, and Si II which are in part due to absorption in high-velocity cloud Complex *C III*. Two sight lines (H1821+643 and 3C 351) which extend through the warped outer Galaxy exhibit strong absorption by singly ionized metals (C II, Si II, Fe II, Mg II) and highly ionized gas (C IV) at velocities corresponding to absorption in the outer Galaxy. Combining our measurements of C IV with data from the literature, we derive a Galactic C IV exponential scale height of 4.9 kpc and a midplane density of 7.1×10^{-9} atoms cm^{-3}. However, the C IV distribution is so patchy that the measurements are found to be equally well fitted by a spherical halo model with a Galactocentric exponential scale length of 6.9 kpc. A comparison of absorption in high-redshift damped Lyα systems with the absorption produced by the Milky Way shows that an appreciable fraction of the damped Lyα absorption-line systems have mixed ionization absorption-line characteristics roughly similar to that found for six sight lines through the Milky Way disk and halo. Since the low-ionization lines are highly saturated, this similarity does not imply similar abundances in the neutral and weakly ionized gas but instead probably suggests a similarity in the kinematical behavior of the different absorbing media.

Subject headings: ISM: abundances — quasars: general — ultraviolet: interstellar

1. INTRODUCTION

The Quasar Absorption Line Key Project is designed to obtain a data base of ultraviolet spectra of quasars to investigate at low and intermediate redshift the absorption produced by galaxy disks and halos including the disk and halo of the Milky Way, by gaseous matter in galaxy clusters and voids, and by the intergalactic medium. In this paper we report on absorption lines found near zero redshift due to Milky Way

[1] Based on observations with the NASA/ESA *Hubble Space Telescope* obtained at the Space Telescope Science Institute, which is operated by the Association of Universities for Research in Astronomy, Inc., under NASA contract NAS 5-26555.

[2] Department of Astronomy, University of Wisconsin, 475 North Charter Street, Madison, WI 53706.
[3] Institute for Advanced Study, School of Natural Sciences, Princeton, NJ 08540.
[4] Institut d'Astrophysique de Paris, CNRS, 98 bis, boulevard Arago, F-75014, Paris, France.
[5] Royal Greenwich Observatory, Madingley Road, Cambridge, CB3 0EZ, England.
[6] Space Telescope Science Institute, 3700 San Martin Drive, Baltimore, MD 21218.
[7] National Radio Astronomy Observatory, 520 Edgemont Road, Charlottesville, VA 22903.
[8] California Institute of Technology, Mail Code 105-24, Pasadena, CA 91125.
[9] Department of Physics and Astronomy, University of Pittsburgh, Pittsburgh, PA 15260.
[10] Observatories of the Carnegie Institution of Washington, 813 Santa Barbara Street, Pasadena, CA 91101.
[11] Center for Astrophysics and Space Sciences, 0111, University of California, San Diego, La Jolla, CA 92093.

disk and halo gas. These lines are numerous because of the high detection sensitivity of ultraviolet resonance absorption lines to small column densities of gas. The Key Project spectra provide the opportunity to sample the Milky Way halo in many directions in order to better understand the distribution and kinematics of the gas at large distances from the Galactic plane. The sensitivity of the resonant metal lines to small column densities will permit a search for the metal-line analog to the H I high-velocity cloud phenomena. The zero-redshift absorption produced by the Milky Way provides important reference data for interpreting metal-line absorption systems seen at higher redshift.

The organization of this paper is as follows: In § 2 we review the Key Project observations and data reductions. In § 3 we evaluate the consequences of the modest resolution of the high-resolution mode of the Faint Object Spectrograph (FOS) for studying Galactic interstellar matter. We also introduce a velocity calibration technique that allows us to improve the accuracy of the velocity zero-point calibration over those provided by the standard Key Project data processing. The Galactic distribution of the objects and their relationship to known high-velocity H I clouds is discussed in § 4. In § 5 we summarize the Milky Way lines detected. In § 6 we report the discovery of high-velocity and very high velocity metal-line clouds. In § 7 we discuss absorption by high-velocity cloud Complex *C* in the direction of PG 1259+593. In § 8 the spectra for H1821+643 and 3C 351 are used to provide information about absorption in the outer warped region of the Milky Way. In § 9 we discuss the implications of the new C IV measurements for estimating the Galactic scale height of C IV. In § 10 we compare the absorption-line characteristics of Milky Way disk and halo gas absorption with absorption seen in higher redshift QSO absorption-line systems. Section 11 provides a brief summary of the study.

2. OBSERVATIONS AND REDUCTIONS

The observations analyzed in this paper are those FOS $\lambda/\Delta\lambda = 1300$ measurements presented by Bahcall et al. (1993a, hereafter Paper I) supplemented with more recent Key Project measurements for two additional quasars including TON 153 and PG 1352+011. The FOS instrumental characteristics, data handling, and processing techniques relevant to the Key Project study are discussed by Schneider et al. (1993, hereafter Paper II). Additional information about the performance of the FOS is found in the *HST* FOS Instrument Handbook (Kinney 1992).

The quasars observed are listed in Table 1. For all the objects, FOS spectra were obtained which extend from 1600 to 2310 Å with grating G190H and from 2230 to 3270 Å with grating G270H. For several objects (3C 273, PG 1259+53, H1821+643, and 3C 351) integrations were also obtained with grating G130H providing spectra extending from 1150 to 1606 Å. The spectra were all obtained through the 0.″25 × 2.″0 slit and recorded with photon-counting 512 channel Digicon detectors. The red Digicon was used for the G190H and G270H integrations, while the blue Digicon was used for the G130H integrations. Four spectrum samples were obtained per Digicon diode width, which approximately corresponds to one resolution element.

The spectra have typical signal-to-noise ratios per resolution element of 25. However, for the bright quasars 3C 273 and H1821+643 the Key Project team reprocessed the guaranteed observing time (GTO) data of Bahcall et al. (1991, 1992). These spectra have signal-to-noise ratios of 30–70 per resolution element.

The spectra for 13 of the 15 quasars analyzed here are displayed in Paper I. Table 6 of that paper contains lists of absorption-line wavelengths and equivalent widths for all lines with minimum equivalent widths 4.5 times the 1 σ equivalent width error for an unresolved line. This line list is referred to as the "complete list." These measurements were performed on continuum normalized spectra as described in Paper II. The equivalent widths were determined by fitting the observed absorption lines with single or, in the case of blends, multiple different width Gaussian profiles. Measurements were also obtained for weaker lines having equivalent widths between 3.0 and 4.5 σ. This list of lines, which will not be published, is referred to as the "incomplete list" in Key Project papers.

3. SPECTRAL RESOLUTION AND VELOCITY CALIBRATION

The spectral resolutions of the FOS high-resolution modes are well described by Gaussian functions with FWHM = 1.1, 1.5, and 2.0 Å for gratings G130H, G190H, and G270H, respectively (see Paper II). At the mid–wavelength range of each grating these resolutions correspond to FWHM (km s^{-1}) = 240, 230, and 220 km s^{-1}, respectively. Some insight into the impact of this resolution for studies of Milky Way and extragalactic absorption is revealed in Figure 1, where we compare the FOS measurements of absorption toward 3C 273 with measurements from the Goddard High-Resolution Spectrograph (GHRS) that have a resolution of approximately 20 km s^{-1} (FWHM) but broad wings on the spectroscopic spread function (see Savage et al. 1993). The figure compares the spectra as a function of LSR velocity with the different spectra in the three panels referenced to the lines of Si II λ1260.42, Fe II λ2600.17, and Mg II λ2796.35. In each panel various other absorption lines also appear, including S II $\lambda\lambda$1253.81 (−1574), 1259.52 (−214), Mn II $\lambda\lambda$2576.88 (−2687), 2594.50 (−644), 2606.17 (+692), Fe II λ2586.65 (−1560), and Mg II λ2803.53 (+770), where the apparent LSR velocities of the other absorption lines are given in parentheses. In most cases the strong lines that FOS detects (Mg II $\lambda\lambda$2803.53, 2796.35, Fe II $\lambda\lambda$2600.17, 2586.65, Si II λ1260.42) represent very strongly saturated absorption features, while the weak lines FOS can detect in the highest quality data represent moderately saturated lines (S II $\lambda\lambda$1253.81, 1259.52, Mn II $\lambda\lambda$2576.88, 2594.50, 2606.46) (see Savage et al. 1993).

The FOS spectra of S II λ1259.52 and Si II λ1260.42, which are −214 km s^{-1} apart, show that the two lines must be farther than 250 km s^{-1} apart before they can be clearly resolved. This blending limits our ability to see and resolve high-velocity metal absorption lines. In some of the absorption profiles that have reliable velocity calibrations, however, high-velocity absorption in the range from 100 to 250 km s^{-1} is evident as an extension of the line profile to positive or negative velocities. Also, for the strong lines of C II, Si II, Mg II, and Fe II, the equivalent widths themselves sometimes imply high-velocity absorption. For example, the Mg II λ2796.35 equivalent width toward H1821+643 of $W_\lambda = 1.73$ Å implies a velocity equivalent width $W_v = W_\lambda c/\lambda = 185$ km s^{-1}. This extremely strong line must have very strong absorption over at least 185 km s^{-1}. In contrast, the Mg II λ2796.35 line toward 3C 273 has $W_v = 115$ km s^{-1}.

In the standard Key Project processing of FOS data, the measurements from the different gratings were brought into a common wavelength system by determining small zero-point

TABLE 1

OBJECT LIST AND VELOCITY CORRECTIONS

QSO	l	b	$v_{lsr} - v_{helio}$ (km s^{-1})	$v_{lsr}(-)$ (km s^{-1})	$v_{lsr}(+)$ (km s^{-1})	Δv (km s^{-1})	$\langle v_{lsr} \rangle$ (km s^{-1})	N(H I) (10^{20} cm^{-2})	E(B-V) mag.	Note
PG 0043+039	120.2	-58.7	-2	-86	+35	121	-26	2.99	0.05	1
PKS 0044+030	120.8	-59.5	-3	-78	+17	95	-31	2.81	0.05	
3C 95	205.5	-46.3	-16	-56	+34	90	-11	4.20	0.07	
US 1867	177.1	+39.9	-2	-60	+38	98	-11	2.62	0.05	
3C 263	134.2	-49.5	-3	-72	+32	104	-20	0.91	0.02	2
3C 273	290.0	+64.4	+2	-62	+46	108	-8	1.68	0.03	
PG 1259+593	120.6	+58.1	+10	-160	+28	188	-66	1.54	0.03	3
TON 153	37.7	+83.7	+9	-64	+36	100	-14	1.27	0.02	
PG 1352+011	335.7	+59.6	+8	-44	+48	92	+2	2.07	0.04	
B2 1512+37	59.9	+58.3	+16	-70	+24	94	-23	1.40	0.02	
3C 351	90.1	+36.4	+16	-86	+37	123	-25	2.02	0.03	4
H 1821+643	94.0	+27.4	+16	-146	+46	192	-50	3.81	0.07	5
PKS 2145+06	63.7	-34.1	+10	-97	+51	148	-23	4.70	0.08	
3C 454.3	86.1	-38.2	+7	-91	+45	136	-23	6.94	>0.12	6
PKS 2251+11	82.8	-41.9	+7	-76	+47	123	-15	5.42	0.09	7

1. PG 0043+039 has an H I HVC at -360 km s^{-1} with N(H I) = 1.9×10^{18} atoms cm^{-2} and FWHM = 41 km s^{-1} (LS93a).

2. For 3C 263 possible H I emission extends to -185 km s^{-1} (LS93a).

3. PG 1259+593 has an H I HVC at -127 km s^{-1} with N(H I) = 6.18×10^{19} atoms cm^{-2} and FWHM = 22 km s^{-1} (LS93a). This HVC is part of Complex *C*.

4. 3C 351.0 has weak H I emission extending from -107 to -198 km s^{-1} with N(H I) = 9×10^{18} atoms cm^{-2} (LS93a). This emission is probably associated with the warp of the outer Galaxy (see § 8). The analysis in the rest of this paper assumes $v_{LSR}(-) = -198$ km s^{-1} and $\langle v_{LSR} \rangle = -80$ km s^{-1}.

5. H1821+643 has very broad H I emission at -99 km s^{-1} with N(H I) = 1.45×10^{19} atoms cm^{-2} and FWHM = 72 km s^{-1} (LS93a). This emission is probably associated with the warp of the outer Galaxy (see § 8).

6. 3C 454.3 has a very faint H I HVC at -369 km s^{-1} with N(H I) = 4.3×10^{17} atoms cm^{-2} and FWHM = 32 km s^{-1} (LS93b). This HVC was not detected in the original survey of LS93a. The sight line to 3C 454.3 intersects a diffuse Galactic molecular cloud that contains sufficient molecules to produce observable CO emission and OH absorption at radio wavelengths (Liszt & Burton 1979; Dickey et al. 1981). The value of $E(B-V)$ based on H I alone $E(B-V)$ is reported as a lower limit.

7. PKS 2251+11 has an H I HVC at -364 km s^{-1} with N(H I) = 4.8×10^{18} atoms cm^{-2} and FWHM = 33 km s^{-1} (LS93a).

8. The wavelength zero-point offsets adopted for TON 153 and PG 1352+11 in the Key Project data processing are as follows:

QSO	G190H	G270H
TON 153	+1.14 Å	+0.33 Å
PG 1352+011	+1.66 Å	+0.82 Å

offsets to the separate spectra based on the assumption that the strong Milky Way metal lines for singly ionized atoms should appear at rest. This assumption is not strictly valid, and improvements to the wavelength scale can be made as described below. The standard zero-point offset mostly relied on the lines Fe II $\lambda\lambda$2600.17, 2586.65, 2382.77 for the G270H grating, the Al II λ1670.79 line (when it was detected) for the G190H grating, and the lines Si II $\lambda\lambda$1526.71, 1304.37, 1260.42, 1193.29, and 1190.42 for the G130H grating. The adopted offsets for each grating are found in Table 3 of Paper I or in the notes to Table 1 of this paper for TON 153 and PG 1352+011. The assumption that the strong lines should be at rest is appropriate for directions where the gas of the Milky Way absorbs relatively symmetrically about $v_{LSR} = 0$ km s^{-1}. However, for some directions high-velocity cloud phenomena may skew the center of the absorption to negative or positive velocities that in extreme cases may approach ± 100 km s^{-1}. For example, in the direction of H1821+643 the 21 cm H I measurements of Lockman & Savage (1993, hereafter LS93a) reveal that H I emission can be traced from $v_{LSR} = -146$ to $+46$ km s^{-1}. If metals exist in the H I emitting gas toward H1821+643, we might expect the strong absorption lines to be centered near $v_{LSR} = -50$ km s^{-1} rather than 0 km s^{-1}.

To improve the velocity zero-point reference of the Key Project data, we have used the H I 21 cm emission-line data of LS93a to estimate a reference velocity, rather than simply assuming that the strong Milky Way lines are at rest. The radio measurements for Key Project quasars reported in LS93a have been corrected for sidelobe contamination in the NRAO 140′ telescope. The strong lines used for the velocity reference are extremely sensitive probes of gas and will be optically thick at all velocities at which 21 cm emission can be detected, provided that the gas contains metals with abundances exceeding approximately 0.1 solar.

In Table 1 we list for each quasar the LSR-to-heliocentric correction, $v_{LSR} - v_{helio}$, and information about Milky Way H I 21 cm emission from LS93a. The negative and positive velocity limits of the observed H I emission, $v_{LSR}(-)$ and $v_{LSR}(+)$, are

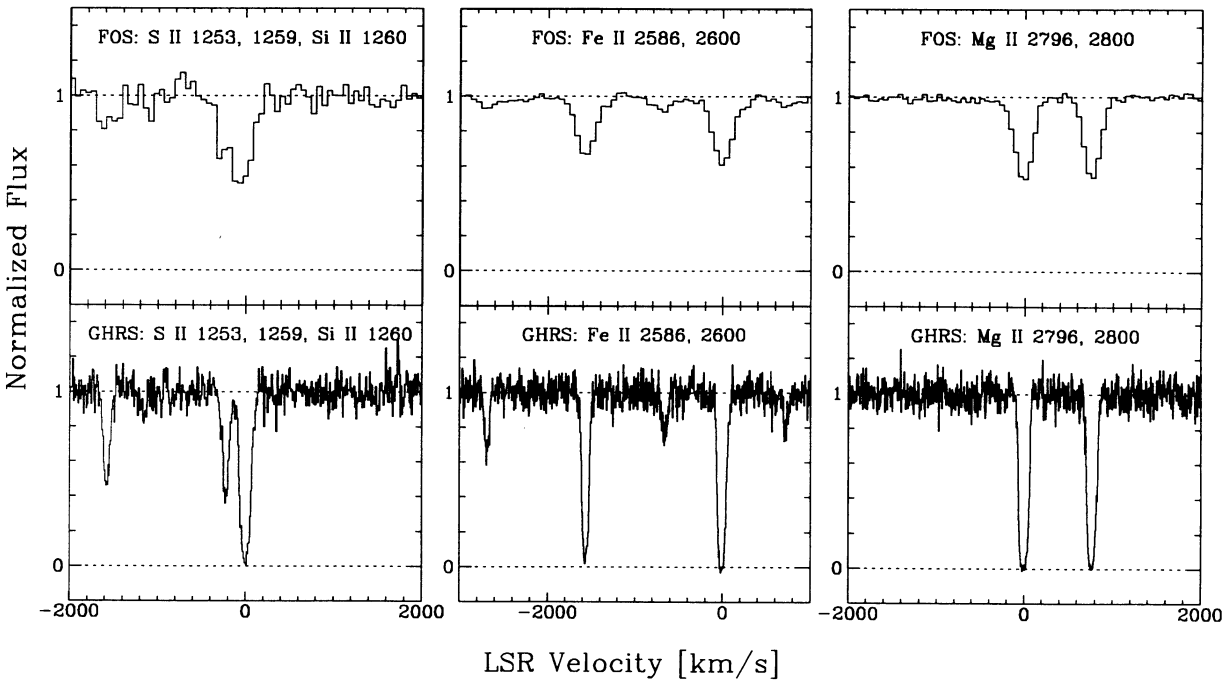

FIG. 1.—Key Project FOS spectra are compared with GHRS spectra from Savage et al. (1993) for selected Milky Way absorption lines toward 3C 273. Continuum normalized intensity is displayed vs. LSR velocity. In the three panels from left to right, the velocity reference is with respect to the lines Si II λ1260.42, Fe II λ2600.17, and Mg II λ2796.35. In each panel various other absorption lines also appear, which include S II λλ1253.81 (at a relative velocity of −1574 km s^{-1}) and 1259.52 (−214) in the left-hand panel; Mn II λλ2576.88 (−2687), 2594.50 (−654), 2606.17 (+692), and Fe II λ2586.65 (−1560) in the center panel; and Mg II λ2803.53 (+770) in the right-hand panel. (In each case the numbers in parentheses are the relative velocities of these lines.)

the limits about zero velocity to which continuous H I emission can be followed above the noise, typically, to an H I brightness temperature of ~0.05 K. Occasionally a completely separate high-velocity component is seen beyond the region defined by $v_{LSR}(-)$ and $v_{LSR}(+)$. These are identified in the notes to Table 1 but not included in the values of $v_{LSR}(-)$ and $v_{LSR}(+)$. The other velocity entries in Table 1 are $\Delta v = |v_{LSR}(+) - v_{LSR}(-)|$ and $\langle v_{LSR}\rangle = [v_{LSR}(+) + v_{LSR}(-)]/2$. As discussed in the next paragraph, the strong absorption lines of species such as C II, Mg II, Si II, and Fe II are expected to be saturated between $v_{LSR}(-)$ and $v_{LSR}(+)$ and, therefore, to have equivalent widths of approximately $W_\lambda = \lambda\,\Delta v/c$ and have average LSR velocities approximately given by $\langle v_{LSR}\rangle$.

The absorption optical depth at velocity v of a species x is given by

$$\tau(v) = (\pi e^2/m_e c) f\lambda N_x(v) = 2.654 \times 10^{-15} f\lambda N_x(v)\,, \quad (1)$$

where the numerical value is for λ in angstroms and the column density per unit velocity, $N_x(v)$, in atoms cm^{-2} (km s^{-1})$^{-1}$. Assuming H I emission to be optically thin, the relation between brightness temperature, T_b (K), and hydrogen column density per unit velocity is

$$N_{H\,I}(v) = 1.823 \times 10^{18} T_b(v) \quad (2)$$

(Spitzer 1978, p. 43). Letting

$$N_x(v) = \delta(x)[X/H]_c\, N_{H\,I}(v)\,, \quad (3)$$

where $\delta(x)$ is the depletion of element x and $[X/H]_c$ is the cosmic abundance ratio of x, and combining equations (1), (2), and (3), we obtain

$$\tau(v) = 4.838 \times 10^3 f\lambda\delta(x)[X/H]_c\, T_b(v)\,. \quad (4)$$

In equation (3) we have assumed that we can convert from the column density of H I per unit velocity to the column density per unit velocity for some other species that represents the dominant ionization state in gas containing H I.

Taking the Mg II λ2796.35 line as an example, with $f\lambda = 1.714 \times 10^3$ (Morton 1991) and $[Mg/H]_c = [Mg/H]_\odot = 3.9 \times 10^{-5}$ (Anders & Grevesse 1989), where the cosmic abundance ratio is taken to be the solar ratio, $[Mg/H]_\odot$, we obtain

$$\tau_{2796}(v) = 323\delta(Mg)T_b(v)\,. \quad (5)$$

Adopting the depletion for Mg found in the lower density warm ISM, $\delta(Mg) = 0.5$ (Jenkins, Savage, & Spitzer 1986), we obtain $\tau_{2796}(v) = 162T_b(v)$. Therefore, an H I brightness temperature limit of 0.05 K implies $\tau_{2796}(v) = 8.1$, and we would expect Mg II λ2796.35 to be fully saturated over the velocity range from at least $v_{LSR}(-)$ to at least $v_{LSR}(+)$. The GHRS Mg II data for 3C 273 (see Fig. 1) show that Mg II λ2796.35 is indeed saturated over a wide velocity range. From Table 1 we find for 3C 273 that $v_{LSR}(-) = -62$ km s^{-1} and $v_{LSR}(+) = +46$ km s^{-1}. Thus, we predict a strong Mg II λ2796.35 line with a velocity width of 108 km s^{-1} centered on $\langle v_{LSR}\rangle = -8$ km s^{-1}. With GHRS we observe a line with a velocity equivalent width $W_v = W_\lambda c/\lambda = 120 \pm 3$ km s^{-1} centered at −5 km s^{-1}. With FOS we observe a line with a velocity equivalent width of 115 ± 5 km s^{-1}. The agreement is encouraging.

Repeating the calculation of $\tau_x(v)$ for the strong lines Fe II λλ2600.17 and 2382.77, we obtain $\tau_{2600}(v) = 91T_b(v)$ and $\tau_{2382}(v) = 112T_b(v)$ using $[Fe/H] = 3.24 \times 10^{-5}$ (Anders & Grevesse 1989) and $\delta(Fe) = 0.04$ (Jenkins et al. 1986). Therefore, $T_b = 0.05$ corresponds to $\tau_{2600}(v) = 4.6$ and $\tau_{2382}(v) = 5.6$, and we would expect the Fe II lines to have a behavior roughly similar to that for Mg II.

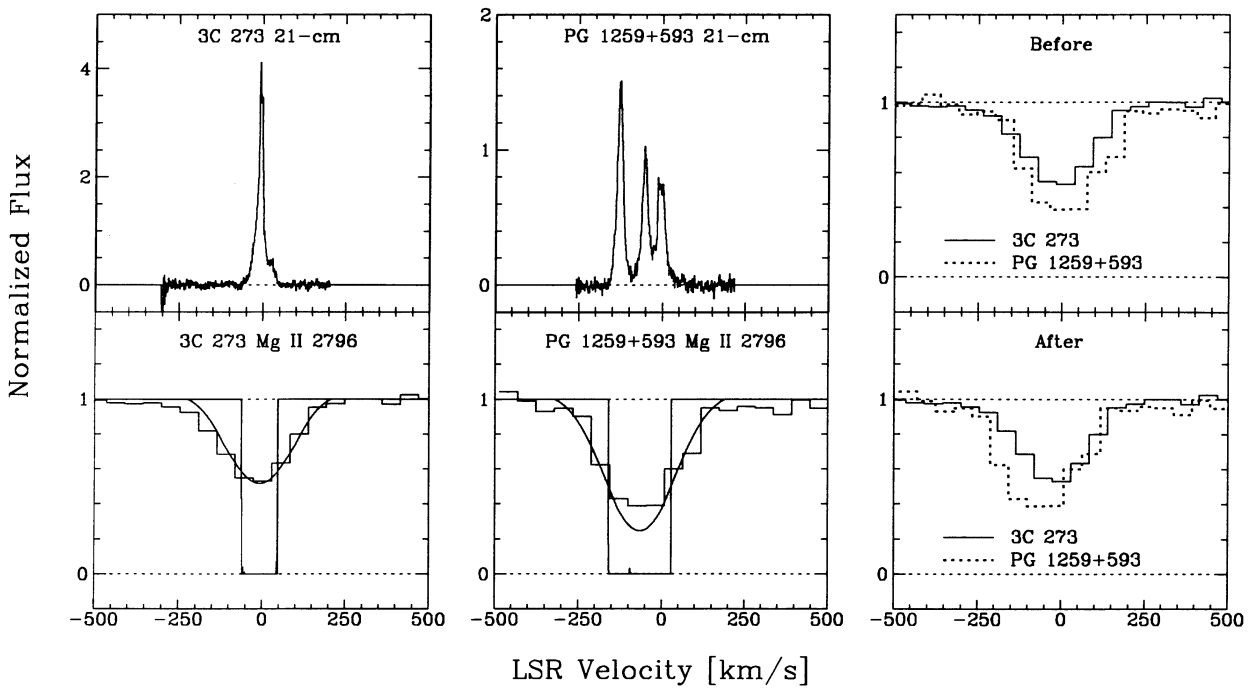

FIG. 2.—An illustration of how the H I 21 cm emission-line measurements of LS93a for the direction to 3C 273 and PG 1259+593 are used to adjust the FOS data into an LSR reference frame. The 21 cm emission (brightness temperature vs. LSR velocity) is shown in the upper part of the left-hand and center panels for 3C 273 (a kinematically simple sight line) and PG 1259+593 (a kinematically complex sight line), respectively. The 21 cm emission is used to predict the strength of Mg II λ2796.53 absorption which would be observed at high resolution and at the FOS resolution. The predicted absorption before and after convolution with the FOS resolution function (*rectangular and smooth curves, respectively*) are compared with the observed absorption (*histogram*) in the panel below each 21 cm emission profile. The comparison has been made following application of the velocity-shifting procedure described in § 3. The right-hand panel compares the Mg II data for the two sight lines before and after the application of the velocity corrections. The much stronger Mg II absorption for the gas toward PG 1259+593 is associated with the high-velocity gas clearly seen in the 21 cm H I emission data toward that quasar. The highest velocity H I emission in that direction ($v_{LSR} \sim -127$ km s^{-1}) is associated with high-velocity cloud Complex *C III* (see § 7).

Figure 2 illustrates the principle behind the velocity adjustment procedure for the Mg II λ2796.35 data for 3C 273 and PG 1259+593. The 21 cm data for the direction to 3C 273 and PG 1259+593 are displayed in the upper half of the two panels to the left, while the lower part of these panels shows the expected shape of the Mg II line if observed at high resolution, and the expected shape if observed at the FOS resolution of 220 km s^{-1} (FWHM). The expected absorption profile at high resolution, $\exp[-\tau(v)]$, was calculated from the H I data using equation (4) with $\delta(\mathrm{Mg}) = 0.5$. Absorption for $v < v_{LSR}(-)$ and $v > v_{LSR}(+)$ was taken to be zero. The expected absorption at FOS resolution, $\exp[-\tau(v)] \otimes \mathrm{SSF}(\Delta v)$, assumes that a Gaussian spectral spread function, SSF(Δv), with FWHM = 220 km s^{-1}, is convolved with the high-resolution absorption profile. The lower panels also show the actual data after application of the velocity offset procedure as described above. The panel on the right shows the FOS data before application of the velocity offset procedure (above) and after application (below). For the direction to 3C 273 the velocity correction only results in a shift of -8 km s^{-1}, while for PG 1259+593 the shift is -66 km s^{-1}. In the direction of PG 1259+593, high-velocity gas associated with high-velocity cloud Complex *C* is evident in the 21 cm emission near $v_{LSR} = -127$ km s^{-1} (see notes to Table 1, and see § 7). That gas is also detected in absorption and causes the strong metal lines to have very large equivalent widths. Note that the velocity equivalent widths for the lines of Mg II and Fe II listed in Table 2 for PG 1259+593 are among the largest out of the group of 15 quasars.

The accuracy of the FOS wavelengths or velocities can be assessed by comparing GHRS and FOS measurements of the Milky Way absorption lines observed toward 3C 273. The GHRS intermediate-resolution measurements from Table 2 of Savage et al. (1993) have an accuracy of ±10 km s^{-1} (1 σ). The comparison includes nine lines for grating G130H and seven lines for grating G270H. By following the procedure discussed above to bring the FOS data into an LSR system, we first adjusted the velocity zero point of the FOS 3C 273 data given in Paper I by -8 km s^{-1}. We then found, for the 16 lines, $\langle v_{LSR}(\mathrm{FOS}) - v_{LSR}(\mathrm{GHRS})\rangle = -12 \pm 17 (1\,\sigma)$ km s^{-1}. The comparison provided no evidence for wavelength-dependent systematic differences that might be associated with errors in FOS dispersion constants. From this comparison we conclude that the FOS wavelength scale is reliable provided that the absolute velocity reference to the Milky Way absorption can be made. This is true for the G130H measurements and the G270H measurements. However, for the G190H measurements only one Milky Way line is available (Al II λ1670.79), and it is not always detected. The FOS 3C 273 data compared here have higher signal-to-noise ratio (S/N) than the typical FOS Key Project data. We estimate that the recalibrated data for representative Key Project spectra will have velocity uncertainties about 35 km s^{-1}, a factor of 2 larger than the rms error of ±17 km s^{-1} measured for the high-quality 3C 273 data set.

Measured absorption-line equivalent widths and their errors for the strong lines of Mg II, λλ2796.35 and 2803.53, and Fe II λλ2600.17 and 2382.77, expressed in velocity units, $W_v = W_\lambda c/\lambda$, are listed in Table 2. These numbers are taken from the

TABLE 2

Fe II AND Mg II ABSORPTION-LINE EQUIVALENT WIDTHS (km s^{-1})

QSO	W_v (km s^{-1})				Δv (km s^{-1})[a]
	Mg II λ2796	Mg II λ2803	Fe II λ2600	Fe II λ2382	H I 21 cm
PG 0043+39	85 ± 11	100 ± 15	108 ± 18	94 ± 15	121
PKS 0044+03	73 ± 11	94 ± 11	93 ± 18	[b]	95
3C 95	98 ± 11	81 ± 12	65 ± 10	72 ± 9	90
US 1867	121 ± 14	96 ± 15	105 ± 16	92 ± 13	98
3C 263	183 ± 14	149 ± 14	127 ± 13	151 ± 18	104
3C 273	115 ± 5	108 ± 1	103 ± 5	103 ± 1	108
PG 1259+593	178 ± 9	189 ± 9	175 ± 12	151 ± 13	188
TON 153	86 ± 10	88 ± 6	82 ± 12	81 ± 8	100
PG 1352+011	107 ± 14	79 ± 9	74 ± 9	76 ± 13	92
B2 1512+37	118 ± 11	110 ± 11	101 ± 10	105 ± 9	94
3C 351	185 ± 13	152 ± 12	112 ± 7	155 ± 16	123
H1821+643	185 ± 5	183 ± 3	173 ± 3	172 ± 4	192
PKS 2145+06	129 ± 14	113 ± 9	173 ± 23	[b]	148
3C 454.3	116 ± 18	111 ± 14	55 ± 10	81 ± 14	136
PKS 2251+11	102 ± 9	87 ± 9	90 ± 14	88 ± 11	123

[a] Velocity extent of H I 21 cm emission from LS93a (see Table 1).

[b] Line not present in the complete sample of lines which satisfy the required 4.5 σ detection significance level.

equivalent width measurements listed in Table 6 of Paper I and do not include high-velocity cloud absorption when it is resolved from the lower velocity absorption (see notes to Table 1). The far right-hand column of Table 2 lists the velocity range Δv over which 21 cm emission has been traced by LS93a (also see col. [7] of Table 1). Figure 3 shows W_v plotted against Δv for the lines of Mg II λ2796.35 and Fe II λ2600.17 for all the objects listed in Table 1. With only a few exceptions, it appears that the measured velocity equivalent widths of the strong metal lines of Mg II λ2796.35 and Fe II λ2600.17 agree well with the expected velocity equivalent widths based on the 21 cm emission toward each quasar. The exceptions are identified with the special symbols in Figure 3. They include 3C 263 (*crosses*), 3C 351 (*plus signs*), and 3C 454.3 (*asterisks*). Note that the measurements do not include absorption produced in very high velocity metal-line clouds which are resolved in the FOS spectra for PG 0043+039, 3C 454.3, and PKS 2251+11.

For 3C 263 and 3C 351 the FOS Mg II λ2796.35 absorption-line equivalent widths are substantially larger than the values of Δv given in Table 1, indicating absorption by gas not accounted for in the 21 cm emission-line data. However, for 3C 263 the 21 cm emission possibly extends to -185 km s^{-1} rather than the quoted value of $v_{\rm LSR}(-) = -72$ km s^{-1} (LS93a). If this emission is real, then Δv for 3C 263 increases from 104 to 217 km s^{-1} and the Mg II discrepancy is removed but is replaced with a discrepancy for Fe II. In the case of 3C 351 the Mg II discrepancy is evidently caused by weak H I emission between -198 and -107 km s^{-1} but not included in the calculated value of Δv listed in Table 1 (see note 4). This problem renders invalid the small LSR (-25 km s^{-1}) velocity correction for 3C 351 listed in Table 1. A more accurate number which will be used elsewhere in this paper $\langle v_{\rm LSR}\rangle = (37 - 198)/2 = -80$ km s^{-1}. For 3C 454.3, the value $W_v = 55 \pm 10$ km s^{-1} for Fe II λ2600.17 is smaller than we

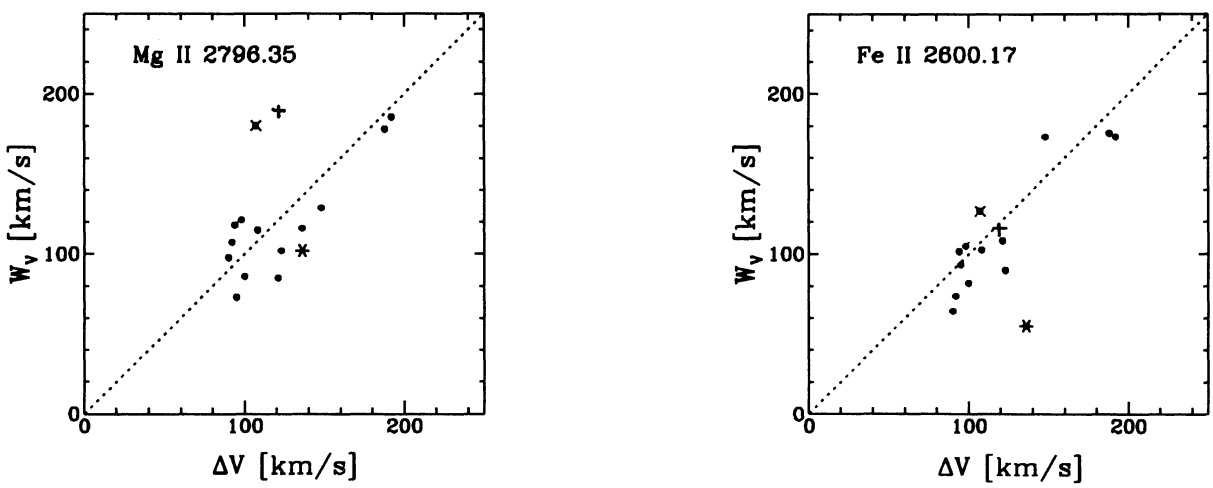

FIG. 3.—Velocity equivalent widths, $W_v = W_\lambda c/\lambda$, for the strong metal lines of Mg II λ2796.35 and Fe II λ2600.17 from Table 2 are compared with the velocity extent, Δv, of measurable H I 21 cm emission from LS93a toward the Key Project quasars. Deviating points are for 3C 263 (*crosses*), 3C 351 (*plus signs*), and 3C 454.3 (*asterisks*). The measured equivalent widths do not include the absorption produced by very high velocity metal-line clouds which are resolved by FOS in the spectra of PG 0043+039, 3C 454.3, and PKS 2251+11. The 1 σ errors in the velocity equivalent widths are typically 10–15 km s^{-1} (see Table 2).

would expect to measure based on $\Delta v = 136$. The discrepancy is somewhat less for the line of Fe II λ2382.77, where we obtain $W_v = 81 \pm 14$ km s^{-1}. It is interesting in this case to find that the agreement is acceptable for both the lines of Mg II (see Fig. 3 and Table 2). Perhaps the higher velocity gas toward 3C 454.3 experiences greater Fe II depletion than the value assumed for the warm interstellar medium (ISM). For all three of these objects we are beginning to see the limitations of the method.

Although the comparison of Figure 3 is not perfect, the fact that the agreement is good for most of the cases suggests that the 21 cm data can be used to improve the velocity zero-point calibration of the FOS data, while the deviant cases suggest that there may occasionally be problems with the calibration scheme and extra care must be taken in these cases. When working with the FOS spectra for Milky Way studies we have adjusted the zero-point wavelengths of the spectra so that the strong metal lines have a velocity given by the values of $\langle v_{\rm LSR} \rangle$ listed in Table 1 (see note for 3C 351). In most cases the adjustment is small (< 35 km s^{-1}). However, in several cases (PG 1259+593, H1821+643, and 3C 351) adjustments as large as -50 to -80 km s^{-1} are required.

There are several reasons why the velocity adjustment technique discussed here will occasionally be invalid. The various Milky Way lines used in the original Key Project data wavelength calibration (see Paper II) have different sensitivities and involve elements with different amounts of depletion due to the presence of dust. Very little is currently known about elemental abundances in high-velocity gas. Also, the 21 cm radio data sample the sky with a 21′ beam. Small angular scale structure in the distribution of the gas can cause the velocity structure seen in absorption, which occurs over an infinitesimal solid angle, to be different from the structure seen in the 21 cm data. Although there is evidence that this effect is not usually important for Milky Way disk gas (Dickey & Lockman 1990), it is likely very important for high-velocity gas (Wakker & Schwarz 1991). The extreme sensitivity of the strong metal lines allows us to sample the sky in a column density regime below an equivalent hydrogen column density of N(H I) = 10^{18} atoms cm^{-2}. Although great care was taken to allow properly for sidelobe contamination in the work reported in LS93a, the resulting H I spectra are somewhat uncertain in the brightness temperature range near 0.05 K. Ionization effects may also introduce differences. Ions such as Si II, Fe II, and Mg II with ionization potentials of 16.34, 16.18, and 15.03 eV, respectively, may produce absorption lines in regions where the hydrogen is ionized. Despite these potential problems, it appears that the H I 21 cm measurements provide a basis for improving the Key Project velocity calibration and for gaining new insights about the nature of the absorption at zero redshift associated with the Milky Way.

4. GALACTIC DISTRIBUTION OF THE QSOs

The Galactic coordinates (l and b) of the 15 quasars included in our study are given in Table 1. Their positions on the sky are shown on the Aittof projection in Figure 4, where the Galactic center is to the right and Galactic longitude increases to the left. Approximately equal numbers are in the northern and southern Galactic hemispheres. The Galactic latitude cutoff of the Key Project quasar absorption line survey ($|b| > 20°$) is evident in the distribution. Key Project quasars were selected on the basis of estimated UV brightness and therefore generally avoid directions with large N(H I) and extinction.

The quasar distribution shown in Figure 4 can be compared with maps of the distribution of high-velocity gas detected via the H I 21 cm emission line (e.g., see Fig. 2 of Wakker 1991). From this comparison we find that four quasars, PG 1259+593, 3C 351, H1821+643, and PKS 2251+11, lie in the direction of high-velocity clouds (HVCs) detected in the data of Wakker (1991). Two other quasars, PG 0043+039 and 3C 454.3, lie near HVCs in the Wakker (1991) map. Because 21 cm emission-line measurements for all sight lines to Key Project quasars observed at higher resolution with FOS are reported in LS93a, we will mostly draw upon their results when discussing the implications of the data for the detection of high-velocity metal-line clouds (see § 6). The notes to Table 1 provide information about those quasars for which high-velocity ($|v_{\rm LSR}| > 100$ km s^{-1}) gas has been detected in the sensitive 21 cm emission measurements of LS93a. In Figure 4

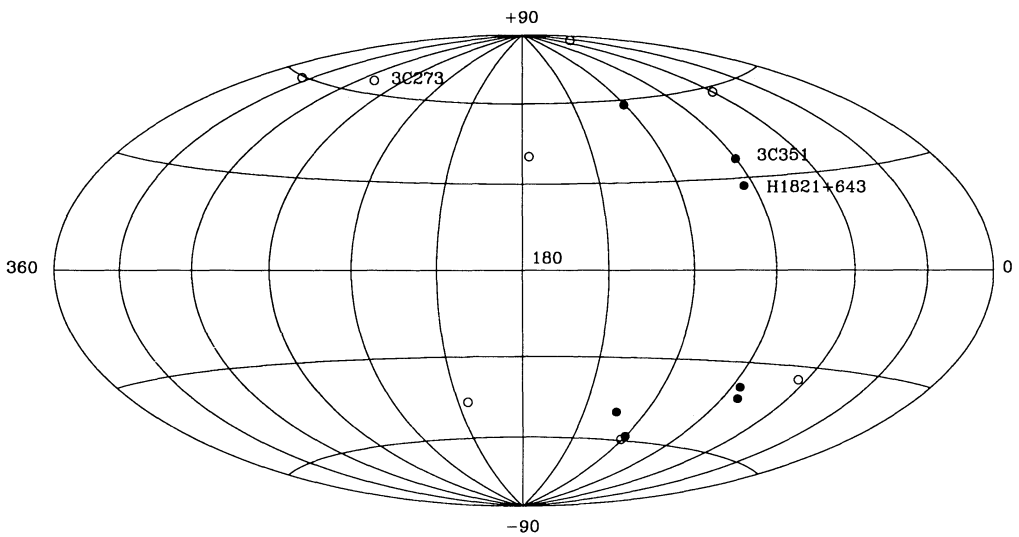

FIG. 4.—Galactic distribution of the Key Project quasars included in this study. In this Aittof projection, the Galactic center is to the right and Galactic longitude increases to the left. Filled symbols mark quasars with high-velocity ($|v| > 100$ km s^{-1}) blended or resolved absorption in the metal lines.

the open circles identify quasars that show no evidence for high-velocity metal-line absorption associated with the Milky Way, while the filled circles identify quasars that do show high-velocity metal-line absorption. 3C 454.3 and PKS 2251+11 lie in directions near the Magellanic Stream (see § 6). PG 1259+593 is in the direction of high-velocity cloud Complex *C* (see § 7). 3C 351 and H1821+643 are in directions which allow us to sample absorption by gas in the outer warped arm of the Milky Way (see § 8).

Estimates of interstellar extinction to the Key Project quasars can be obtained from the 21 cm emission-line data and the assumption that the standard value of N(H I)/$E(B-V) = 5.7 \times 10^{21}$ atoms cm^{-2} mag^{-1} (Bohlin, Savage, & Drake 1978) is valid. The resulting estimates of the reddening, $E(B-V)$, are listed in column (10) of Table 1. These estimates can be used along with an assumed shape for the UV interstellar extinction curve (Savage & Mathis 1979; Cardelli, Clayton, & Mathis 1989) to correct the observed QSO energy distributions for the effects of UV interstellar extinction. In general, the extinction will be relatively small because quasars in directions with large N(H I) were biased against in the Key Project object selection. A possible exception is 3C 454.3, which apparently lies behind a diffuse molecular cloud (Liszt & Burton 1979; Dickey, Crovisier, & Kazes 1981). The radio data are not sufficient to determine the $N(H_2)$ for this cloud, but by analogy with other clouds the visual extinction A_V may exceed 0.3 mag and is possibly as high as 1 mag in this component alone (Turner 1988).

5. MILKY WAY HALO ABSORPTION LINES

Table 3 lists the Galactic absorption lines expected to be detectable in high S/N FOS spectra. The vacuum wavelengths in Å and values of log [λ(Å)f] are from Morton (1991). In a number of cases the feature indicated is a blend of lines, as noted in the notes to the table. The list is for those lines expected to have equivalent widths exceeding approximately 0.1 Å when viewing at Galactic latitude $|b| > 20°$. The list is similar to that in Paper I (Table 7) and in Savage (1988), which was based on results obtained with the *International Ultraviolet Explorer* (*IUE*) of absorption toward stars in the low halo and for the sight lines to the Large and Small Magellanic Clouds.

The FOS Key Project equivalent width measurements for Milky Way absorption toward 3C 273, H1821+643, 3C 351, and PG 1259+593 are also listed in Table 3, along with the 1 σ errors in those measurements. These are the four quasars for which data are available from all three gratings. The listed lines are from the Key Project complete list and have significance levels exceeding 4.5 σ. The high signal-to-noise ratio GTO measurements of Bahcall et al. (1991, 1992) for 3C 273 and H1821+643 represent the highest quality data we expect to obtain in the Key Project survey and can be used as a guide in assessing the strong and weak absorption lines that might be expected to be present along other sight lines. Absorption in 34 and 31 different Milky Way lines is evident toward 3C 273 and H1821+643, respectively. The measurements for 3C 351 and PG 1259+593 are more representative of the typical Key Project data, having signal-to-noise ratios of approximately 25 per diode. For 3C 351 and PG 1259+593, the Key Project absorption-line search routines identify absorption in 15 and 18 Milky Way lines, respectively (see Table 6 of Paper I).

The Milky Way lines detected are numerous and strong. Toward the 13 quasars observed at $\lambda/\Delta\lambda = 1300$ resolution and analyzed in Paper I, 44% of the identified absorption lines are from the Milky Way. The strongest low-ionization lines found in the data for 3C 273 and H1821+643 include those of H I, C II, O I, N I, Mg II, Fe II, Si II, and Al II. Lines of intermediate ionization including Si III and Al III are also seen. The high-ionization lines found in the FOS data are from C IV and Si IV. In the case of H1821+643, the Milky Way Si IV lines are probably present, but they are badly blended with intergalactic Lyα absorption (see Paper I and § 8). Absorption by N V, which is an important tracer of hot interstellar gas, is difficult to see with the resolution and signal-to-noise ratio of the FOS data. The N V $\lambda\lambda$1238.82, 1242.80 doublet was seen toward 3C 273 with the GHRS (Morris et al. 1991; Savage et al. 1993) with $W_\lambda = 0.126 \pm 0.023$ and 0.071 ± 0.024 Å, respectively. Features of low statistical significance ($\sim 2\,\sigma$) attributed to N V were also reported by Bahcall et al. (1991). The strong neutral and singly ionized metal lines observed in the spectrum of H1821+643 are about 1.5 times stronger than for 3C 273, while the high-ionization lines of C IV have comparable strength for the two objects.

When data are available only for gratings G190H and G270H, the Key Project data set typically contains nine Milky Way absorption lines from the species Mg I λ2852.96, Mg II $\lambda\lambda$2803.53, 2796.35, Fe II $\lambda\lambda$2600.17, 2586.65, 2382.77, 2374.46, 2344.21, and Al II λ1670.79 (see Table 6 of Paper I).

6. DETECTION OF HIGH-VELOCITY AND VERY HIGH VELOCITY METAL-LINE CLOUDS

Ultraviolet resonance lines of abundant atoms with large oscillator strengths are extremely sensitive probes of gas. The Quasar Absorption Line Key Project higher resolution data base contains G270H and G190H observations for all the quasars listed in Table 1 and coverage with G130H for four quasars. Thus, the lines most suitable for a search for metal-line analogs to the H I 21 cm high-velocity cloud phenomena are the strongest lines included in the spectral region from approximately 1600 to 3200 Å. Candidate lines include Mg II $\lambda\lambda$2796.35 and 2803.53, Fe II $\lambda\lambda$2382.77 and 2600.17, and Al II λ1670.79. The detection sensitivity is influenced by the product of wavelength, f-value, and element abundance along with the S/N in the FOS spectra at the relevant wavelengths. For the G270H and G190H spectra obtained so far, the S/N is best for the lines of Mg II and worst for the line of Al II. Using the solar Mg, Fe, and Al abundances from Anders & Grevesse (1989) of $(X/H)_\odot = 3.89 \times 10^{-5}$, 3.23×10^{-5}, and 3.02×10^{-6}, respectively, we obtain values of λf(X/H) = 0.067, 0.033, 0.023, 0.019, and 0.0092, respectively, for the above-mentioned lines of Mg II, Fe II, and Al II. The depletion of an element onto dust will reduce the detection sensitivity. This effect will be particularly severe for Fe and Al (Jenkins 1989). We conclude that the combination of atomic physics, abundance, and S/N in the spectra implies that the most sensitive lines are those of Mg II $\lambda\lambda$2796.35 and 2803.53.

We display in Figure 5 the continuum normalized absorption-line profiles for the lines Fe II $\lambda\lambda$2586.65 and 2600.17 and Mg II $\lambda\lambda$2796.35 and 2803.53 for all the quasars listed in Table 1. The profiles have been plotted on an LSR velocity basis with $v_{LSR} = 0$ km s^{-1} referenced to Fe II λ2600.17 in the panels to the left and to Mg II λ2796.35 in the planes to the right. With this form of presentation Fe II λ2586.56 appears at -1560 km s^{-1} in the panels to the left, while Mg II λ2803.53 appears at $+770$ km s^{-1} in the panels to the right. In the high signal-to-noise ratio measurements for 3C

273 and H1821+643, the weak lines Mn II λλ2576.88, 2594.50, 2606.17 are also apparent in the left-hand panel at v_{LSR} = −2687, −654, and +692 km s^{-1} (also see discussion of Fig. 1 in § 3).

The FOS resolution of 220 km s^{-1} limits our ability to resolve HVCs unless they have large velocities. However, high-velocity absorption between 100 and approximately 220 km s^{-1} blended with absorption by low-velocity gas is evident for some of the sight lines. The large velocity equivalent widths for the strongest absorption lines for these sight lines implies that there is gas with $|v_{LSR}| > 100$ km s^{-1}. Table 4 lists those quasars for which we see in the FOS spectra either resolved high-velocity absorption (three cases) or high-velocity absorption blended with absorption from lower velocity gas (four cases).

Table 4 also contains information about high-velocity H I emission as measured by LS93a and Lockman & Savage (1993b, hereafter LS93b) toward each quasar with the NRAO 140′ radio telescope. The various entries are v_{pk}, the peak velocity of the emitting cloud, the FWHM of the Gaussian fit

TABLE 3

MILKY WAY LINES

Ion	λ (vac)	log λf	$W_\lambda \pm 1\sigma$ 3C 273		$W_\lambda \pm 1\sigma$ H 1821+643		$W_\lambda \pm 1\sigma$ 3C 351		$W_\lambda \pm 1\sigma$ PG 1259+593		note
Mg I	2852.96	3.718	0.39	0.05	0.59	0.02	0.59	0.08	0.64	0.11	
Mg II	2803.53	2.933	1.01	0.01	1.71	0.03	1.42	0.11	1.76	0.08	
Mg II	2796.35	3.234	1.07	0.05	1.73	0.05	1.73	0.12	1.66	0.08	
Mn II	2606.46	2.701	0.14	0.02	0.20	0.03	...	...	...	...	
Fe II	2600.17	2.765	0.89	0.04	1.50	0.03	0.97	0.06	1.52	0.10	
Mn II	2594.50	2.847	0.20	0.02	0.30	0.04	...	...			
Fe II	2586.65	2.223	0.79	0.02	1.06	0.03	0.63	0.07	1.02	0.11	
Mn II	2576.88	2.956	0.14	0.02	0.39	0.04	...	...			
Fe II	2382.77	2.855	0.82	0.01	1.37	0.03	1.23	0.13	1.20	0.10	
Fe II	2374.46	1.826	0.60	0.02	1.03	0.05	0.74	0.20	0.67	0.07	
Fe II	2344.21	2.410	0.71	0.01	1.04	0.10	0.83	0.09	1.15	0.12	
Fe II	2260.78	0.924	...	...	0.27	0.05	...	...	...	...	
Fe II	2249.88	0.752	0.12	0.03	0.25	0.03	...	...	...	...	
Zn II	2062.66	2.717	0.29	0.04	0.17	0.03	..	...	...	...	1
Zn II	2026.14	3.018	0.28	0.02	0.17	0.03	...	...	...	...	2
Al III	1862.79	2.716	0.15	0.02	...	...	...	...	...	...	
Al III	1854.72	3.017	0.19	0.02	0.30	0.05	...	...	...		
Si II	1808.01	1.000	...	....	0.25	0.04	...	...	0.34	0.05	3
Al II	1670.79	3.486	0.56	0.03	0.83	0.05	0.63	0.04	0.73	0.08	
C IV	1550.77	2.169	0.39	0.02	0.36	0.03	...	...	0.14	0.02	
C IV	1548.20	2.470	0.54	0.01	0.53	0.03	0.45	0.03	0.28	0.02	
Si II	1526.71	2.546	0.49	0.02	0.74	0.03	0.67	0.03	0.71	0.03	
Si IV	1402.77	2.554	0.29	0.01	...	...	...	...	...	...	
Si IV	1393.76	2.855	0.51	0.01	...	...	...	...	...	...	
C II*	1335.71	2.186	0.18	0.02	...	...	...	...	...	...	
C II	1334.53	2.232	0.62	0.01	0.83	0.02	1.04	0.05	1.04	0.05	4
Si II	1304.37	2.284	0.40	0.02	0.81	0.05	...	...	...	...	
O I	1302.17	1.804	0.41	0.01	0.85	0.05	...	...	...	...	5
Si II	1260.42	3.104	0.55	0.03	1.36	0.05	1.01	0.05	1.07	0.06	6
S II	1259.52	1.311	0.28	0.03	...		...	...	...	...	6
S II	1253.81	1.135	0.20	0.02	0.39	0.04	0.93	0.07	...	...	
S II	1250.58	0.834	...	...	...	...	...	...	...	...	7
N V	1242.80	1.988	...	...	...	...	...	...	...	...	8
NV	1238.82	2.289	...	...	...	...	...	...	...	...	8
H I	1215.67	2.704	...	...	...	...	...	...	...	...	9
Si III	1206.50	3.304	0.57	0.02	0.67	0.10	0.86	0.11	0.88	0.14	
N I	1199.97	2.503	1.02	0.03	0.99	0.09	...	...	...	...	10
Si II	1193.29	2.775	0.50	0.03	0.66	0.07	...	...	0.79	0.14	
Si II	1190.42	2.474	0.55	0.03	1.15	0.13	...	...	...	...	11

NOTES TO TABLE 3

1. Zn II λ2062.66 blends with Cr II λ2062.23.
2. Zn II λ2026.14 blends with Mg I λ2026.48.
3. Si II λ1808.01 is detected toward 3C 273 with the GHRS with W_λ = 0.136 Å (Savage et al. 1993).
4. For 3C 273 separate measurements are reported for C II* λ1335.71 and C II λ1334.53. For the others the blended measurement is reported under the entry for C II λ1334.53.
5. The interstellar O I λ1302.17 measurement is contaminated by Earth atmospheric O I emission.
6. For 3C 273 separate measurements are reported for Si II λ1260.42 and S II λ1259.52. For the rest the blended measurement is reported under the entry for Si II λ1260.42.
7. S II λ1250.58 is detected toward 3C 273 with the GHRS with W_λ = 0.160 Å (Savage et al. 1993).
8. N V λλ1242.80 and 1238.82 are detected toward 3C 273 with the GHRS with W_λ = 0.071 and 0.128 Å, respectively (Savage et al. 1993).
9. Milky Way damped H I Lyα is present but contaminated with geocoronal Lyα emission. The contamination is severe for 3C 351 and PG 1259+593.
10. The N I absorption is from a closely spaced triplet with lines at 1199.55, 1200.22, and 1200.71 Å. The value of log λf listed is for the multiplet.
11. Si II λ1190.42 is probably blended with S III λ1190.21.

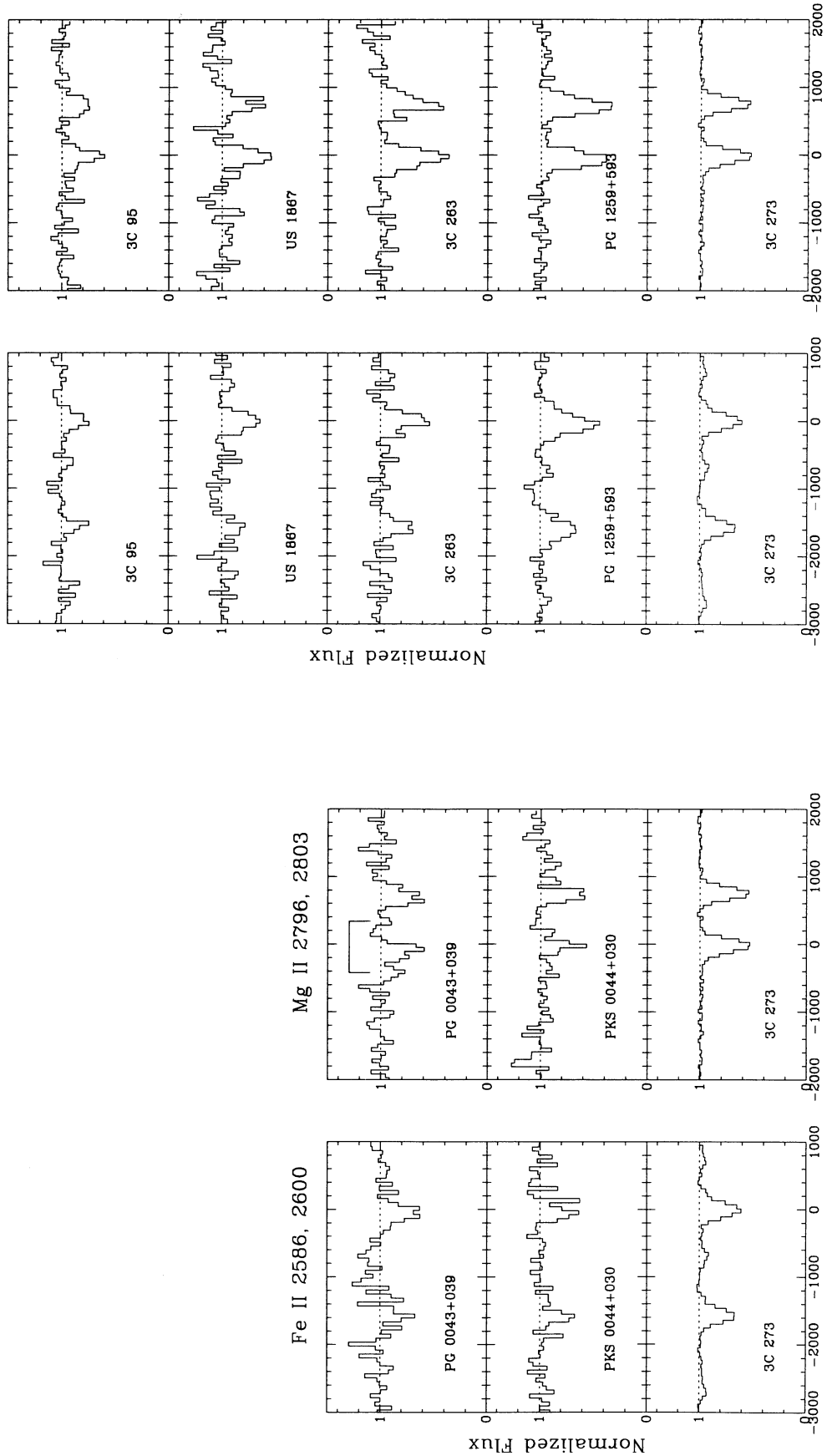

FIG. 5.—Galactic absorption by Fe II and Mg II is shown for all the Key Project quasars listed in Table 1. Continuum normalized intensity is plotted against LSR velocity. In the panels on the left the velocity reference is with respect to Fe II λ2600.17, therefore Fe II λ2586.65 has an apparent velocity of -1560 km s^{-1}. In two cases (3C 273, H1821+643) the measurements have high enough signal-to-noise ratio to also reveal absorption in the triplet of Mn II $\lambda\lambda$2576.88, 2594.50, and 2606.17 at apparent velocities of -2687, -654, and $+692$ km s^{-1}. In the panels on the right the velocity reference is with respect to Mg II λ2796.35. In this case Mg II λ2803.53 absorption occurs at an apparent velocity of $+770$ km s^{-1}. In each of the panels comprising this figure the data for 3C 273 are repeated to illustrate high-quality data for a Galactic sight line with relatively simple kinematical properties (see Fig. 1). Resolved very high velocity absorption in the Mg II doublet is apparent for PG 0043+039, 3C 454.3, and PKS 2251+11. This very high velocity absorption is indicated by brackets in the figure. Quasars having very strong Galactic absorption in the Mg II doublet include 3C 263, PG 1259+593, 3C 351, and H1821+643. In one case (PG 1352+11) the panel containing the Galactic Fe II $\lambda\lambda$2600.17 and 2586.65 absorption also reveals a strong high-redshift C IV doublet ($z = 0.668$).

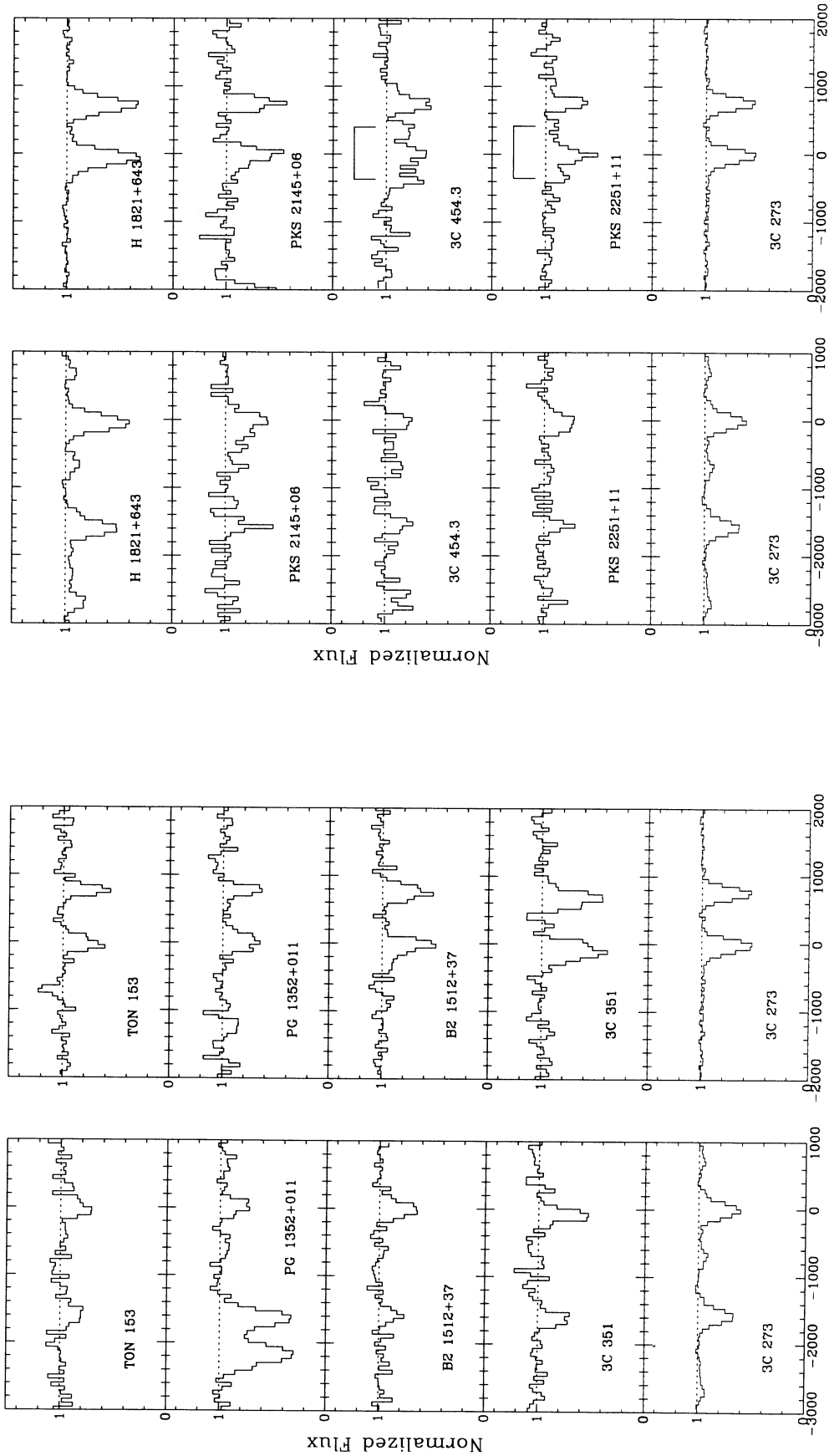

FIG. 5—*Continued*

TABLE 4

HIGH-VELOCITY METAL-LINE ABSORPTION ($|v_{LSR}| > 100$ km s^{-1})

	H I			Mg II					
QSO	v_{pk} (km s^{-1})	FWHM (km s^{-1})	N(H I) (10^{19} cm^{-2})	$v \pm \sigma$ (km s^{-1})	$W_\lambda(2796) \pm \sigma$ (Å)	$W_\lambda(2803) \pm \sigma$ (Å)	N(Mg II) (10^{12} cm^{-2})	$\frac{N(\text{Mg II})}{N(\text{H I})}$ $\frac{}{(Mg/H)_\odot}$	Note
PG 0043+039	−360	41	0.19	−348 ± 41	0.38 ± 0.11	...	>9.0	>0.12	1
3C 454.3	−367	45	0.12	−397 ± 23	0.65 ± 0.10	0.54 ± 0.10	>15	>0.32	1
PKS 2251+11	−364	33	0.48	−374 ± 27	0.43 ± 0.08	0.27 ± 0.12	>11	>0.059	1
3C 263	...	...	...	B[a]	B	B	B	...	2
PG 1259+593	−127	22	6.18	B	B	B	B	...	3
3C 351	−180:	(−198 to −107)	0.90	B	B	B	B	...	4
H1821+643	−99	72	1.45	B	B	B	B	...	4

[a] The B denotes that the high-velocity H I feature is inferred in Mg II and other absorption lines, but it is blended with absorption by lower velocity gas.

NOTES TO TABLE 4

1. The velocity v listed for the high-velocity Mg II absorption is determined from the observed relative velocity offset, v_{rel}, between the principal Mg II absorption component and the high-velocity Mg II absorption. The relative velocity offset was determined from Gaussian profile fitting to the FOS data using the Key Project software (see Paper II). The velocity listed is the sum of v_{rel} and the expected LSR velocity of the principal absorption component based on the 21 cm emission measurements of LS93a. The expected LSR velocity of the principal absorption is simply $\langle v_{LSR} \rangle$ from Table 1. The velocity errors listed for the Mg II high-velocity absorption are determined from the uncertainty associated with the Gaussian component fitted to the data (see Paper II).

2. For 3C 263, H I 21 cm emission may extend to −185 km s^{-1} (LS93a). The discrepancy between W_v and Δv noted in § 3 suggests that the emission does extend to substantial negative velocities. If $v_{LSR}(-)$ is −185 km s^{-1} rather than −72 km s^{-1} as reported by LS93a, the discrepancy is removed.

3. For PG 1259+593 the −127 km s^{-1} HVC is associated with Complex *C*. The HVC is seen in absorption in the lines of Mg II, Fe II, Si II, and C II blended with absorption by lower velocity gas (see § 7).

4. The strong ultraviolet absorption lines seen toward 3C 351 and H1821+643 are caused by absorption associated with the warped outer Galaxy blending with absorption produced in lower velocity gas (see § 8).

to the emission, and N(H I), the H I column density assuming the emission to be optically thin. The HVCs do not always appear as a well-defined component, so v_{pk} and the FWHM are sometimes only approximate (e.g., H1821+643). There is no well-separated high-velocity H I emission component toward 3C 263. A −395 km s^{-1} emitting cloud toward 3C 454.3 was not detected in the LS93a survey, but a cloud with a velocity of −367 km s^{-1} did appear in a very high sensitivity follow-up investigation (LS93b). The column density for that emission (1.2×10^{18} atoms cm^{-2}) is small.

Resolved high-velocity absorption is evident in the strong line of the Mg II doublet, Mg II λ2796.35, at a greater than 3 σ level of significance for PG 0043+039, 3C 454.3, and PKS 2251+11. The corresponding weaker Mg II λ2803.53 lines are seen for both 3C 454.3 and PKS 2251+11. In the case of PKS 2251+11 the Mg II λ2803.53 feature is below the 3 σ significance level. These high-velocity absorption features are indicated on the Mg II profiles shown in Figure 5. The measured LSR velocities, v_{LSR}, equivalent widths, and associated 1 σ errors for the high-velocity Mg II absorption components are listed in Table 4. These measurements are from Gaussian profile fitting to the Mg II absorption using the Key Project software described in Paper II (also see note 1 of Table 5). These resolved high-velocity absorptions are not evident in the strong lines of Fe II or Al II, consistent with the discussion above where we conclude that the Mg II lines are indeed the most sensitive tracer of low column density gas in the spectral region covered by the G190H and G270H gratings.

Lower limits to the column density of Mg II in the very high velocity gas toward PG 0043+039, 3C 454.3, and PKS 2251+11 are listed in Table 4. These limits were obtained from the equivalent width for the stronger line, λ2796.35, of the Mg II doublet assuming no line saturation and using the Mg II oscillator strength $f = 0.612$ from Morton (1991). The detected clouds have lower limits to the Mg II column density ranging from 9.0×10^{12} to 1.5×10^{13} atoms cm^{-2}.

The sight lines to PKS 2251+11 and 3C 454.3 are separated by approximately 5°. According to the high-velocity cloud map in Figure 2 of Wakker (1991), PKS 2251+11 lies in the direction of the Magellanic Stream, and 3C 454.3 is close to the limiting 2×10^{18} atoms cm^{-2} contour for the Magellanic Stream.

The sight line to PG 0043+039 ($l = 120.^\circ2$, $b = -58.^\circ7$) lies close to high-velocity cloud 532 centered on $l = 118.^\circ3$ and $b = -58.^\circ0$ identified in the survey of Wakker & van Woerden (1991). Cloud 532 has a surface area of 2.1 square degrees, an average velocity of −372 km s^{-1}, and a maximum brightness temperature of 0.53 K. The velocity is close to the value −360 km s^{-1} seen in the radio data of LS93a for the direction to PG 0043+039. It is interesting that another observed quasar (PKS 0044+030), which lies 1° away from PG 0043+039, does not show detectable high-velocity Mg II absorption (see Fig. 5) or high-velocity H I emission (LS93a).

The important question of the elemental abundances in very high velocity gas is addressed in column (9) of Table 4, where we list values of $[N(\text{Mg II})/N(\text{H I})]/[\text{Mg/H}]_\odot$. Here $[\text{Mg/H}]_\odot = 3.89 \times 10^{-5}$ is the solar Mg-to-H abundance ratio from Anders & Grevesse (1989). Mg II is the dominant ionization state of Mg in the neutral hydrogen regions of the Milky Way, since the conversion of Mg I into Mg II requires only 7.64 eV, while the conversion of Mg II to Mg III requires 15.03 eV. However, substantial amounts of Mg II can exist in regions where the hydrogen is mostly ionized. Another issue of concern is that the absorption measurements occur over the extremely small solid angle of the background quasar, while the 21 cm emission results for H I provide information about the H I averaged over the 21′ diameter beam of the NRAO 140′ telescope. With these qualifications in mind, the results for $[N(\text{Mg II})/N(\text{H I})]/[\text{Mg/H}]_\odot$ listed in Table 4 imply that the very high velocity gas toward these three quasars has Mg abundances with lower limits ranging from 0.059 solar to 0.32 solar.

From observations with the Westerbork Synthesis Radio Telescope at an angular scale of 1′, Wakker & Schwarz (1991) have found that the HVC phenomena often have small-scale structure. The factor of 5 column density contrast they found for several HVC fields over arcminute angular scales implies that clumping presents a major problem in establishing abundances which are referenced to H I for the HVC phenomena. Reliable abundance studies and even abundance limits for HVCs will probably require 21 cm observations with synthesis telescopes operating at high angular resolution.

The metal-line absorption spectra of four quasars have high-velocity absorption blended with low-velocity absorption. This blended absorption is recognized either from the very large equivalent widths found for the strongest metal lines or from asymmetric extensions of the line profiles for cases where the FOS data are of very high quality. Three of these cases of blended high-velocity absorption are discussed in more detail in §§ 7 and 8. In § 7 the data for PG 1259+593 are used to gain insights about ultraviolet absorption occurring in high-velocity cloud Complex *C*. In § 8 the data for H1821+643 and 3C 351 are used to study high-velocity absorption which is probably associated with the outer warped arm of the Milky Way. Here we briefly comment on the results for 3C 263 and discuss the implications of the fact that we detect metal-line absorption by high-velocity or very high velocity gas toward seven of 15 quasars.

The Milky Way lines of Mg II seen toward 3C 263 are very strong (see Fig. 5). The velocity equivalent width for λ2796.35 is 183 ± 14 km s^{-1}, while Δv(H I) from LS93a is 104 km s^{-1}. However, the radio data did reveal the possible existence of weak H I emission for the sight line to 3C 263 extending to -185 km s^{-1}. If that emission is real, Δv(H I) for 3C 263 increases from 104 to 217 km s^{-1}. This larger Δv(H I) is consistent with the large equivalent width for Mg II λ2796.35. We believe the H I emission probably is real and that the Mg II line for 3C 263 is strong because it is produced by absorption in low-velocity gas blended with that occurring in high-velocity gas.

The Quasar Key Project measurements of the 15 objects listed in Table 1 reveal three cases of very high velocity metal-line absorption and four cases of high metal-velocity metal-line absorption (see Table 4). With seven of 15 sight lines exhibiting either high-velocity or very high velocity metal-line absorption, it would be tempting to conclude that ~47% of the sky is covered by such absorbing clouds. A similar sky-covering calculation performed with the sensitive 21 cm H I survey data of LS93a for the same directions reveals five high-velocity or very high velocity H I clouds (PG 0043+039, PKS 2251+11, PG 1259+593, 3C 351, and H1821+643) toward the 15 quasars, or a ~33% covering factor. For 3C 454.3 H I emission was found through an extremely sensitive H I search conducted after knowing that Mg II absorption was present. In the case of 3C 263 the original LS93a survey data reveal possible high-velocity H I emission. The FOS $\lambda/\Delta\lambda \sim 1300$ resolution data evidently have greater sensitivity to the detection of high-velocity cloud phenomena than most existing H I 21 cm high-velocity cloud surveys.

From an analysis of the sensitive all-sky H I survey measurements of HVCs by Bajaja et al. (1985) and Hulsbosch & Wakker (1988), Wakker (1991) concluded that 18% of the sky is covered with gas having $|v_{\rm LSR}| > 100$ km s^{-1} and N(H I) $> 10^{18}$ atoms cm^{-2}. However, from an extrapolation he estimated that 30%–60% of the sky may be covered with high-velocity gas having N(H I) $> 2 \times 10^{17}$ atoms cm^{-2}. The number given above for the first 15 Key Project sight lines suggests that Wakker's extrapolation may be correct and that the high-velocity gas contains heavy elements.

The measurements of high-velocity and very high velocity gas toward 3C 263 and 3C 454.3 illustrate well the extreme sensitivity of UV resonance absorption-line data to small amounts of gas. Even though the FOS data have only modest resolution (220–250 km s^{-1}), the measurements easily reveal high-velocity absorption that did not appear as certain detections in the sensitive H I survey measurements of LS93a. Future Key Project data are necessary to improve the detection statistics for metal-line analogs to the high-velocity cloud phenomena and to actually determine the sky-covering factor of the metal-line clouds.

7. ABSORPTION BY HIGH-VELOCITY CLOUD COMPLEX *C*

The sight line to PG 1259+593 is in the direction of high-velocity cloud Complex *C*, which was discovered by Hulsbosch & Raimond (1966). Complex *C* is more than 90° long and varies in width between about 10° and 25°. For a short overview of its properties and maps of its angular extent see Wakker & van Woerden (1991). Complex *C* is composed of overlapping substructures (*C I*, *C II*, and *C III*) involving intermediate- and high-velocity gas (Hulsbosch 1968; Danly 1989). In this paper we will indicate high-velocity cloud Complex *C* and its subcomponents in italics in order to avoid confusion with the ions of carbon (C I, C II).

Hydrogen 21 cm emission in the direction of PG 1259+593 is shown in the upper middle panel of Figure 2. Complex *C III* shows up as strong H I emission peaking near -127 km s^{-1} and containing N(H I) $= 6.18 \times 10^{19}$ atoms cm^{-2} (see notes to Table 1). Emission by intermediate-velocity gas probably associated with Complex *C II* is also evident. That emission is characterized by $v_{\rm LSR} = -52$ km s^{-1} and N(H I) $= 4.29 \times 10^{19}$ atoms cm^{-2}. The total integrated H I column density in the direction of PG 1259+593 is 15.4×10^{19} atoms cm^{-2}. Therefore, the H I emission is approximately equally distributed between that associated with Complexes *C III* and *C II* and the low-velocity emission. Through high-resolution ultraviolet absorption-line observations with the *IUE* toward several halo stars Danly (1989) has established that in several directions Complexes *C I* and *C III* are more distant than about 1.7 kpc from the Galactic plane, while *C II* is closer than 1.7 kpc (see also Danly et al. 1992).

The FOS data for PG 1259+593 reveal very strong absorption lines which imply absorption by gas at high velocity. For example, the velocity equivalent widths for the lines of C II λ1334.53, Fe II λ2600, and Mg II λ2796 are 233, 175, and 178 km s^{-1}, respectively. The value for C II λ1334.53 may include some blending from C II* λ1335.70. The large equivalent widths imply strong absorption over a wide velocity range. From the 21 cm emission-line data we would expect strong saturated absorption toward PG 1259+593 over a range of velocity $\Delta v = 188$ km s^{-1}, provided that the high-velocity gas in the direction of PG 1259+593 contains heavy elements with moderate depletions.

Figure 6*a* provides a comparison of the ultraviolet absorption toward PG 1259+593 with that toward 3C 273 for various strong ultraviolet lines. The data for PG 1259+593 and 3C 273 have been velocity-shifted according to the procedure discussed in § 3. The PG 1259+593 measurements are illustrated with heavy lines, while the 3C 273 measurements are

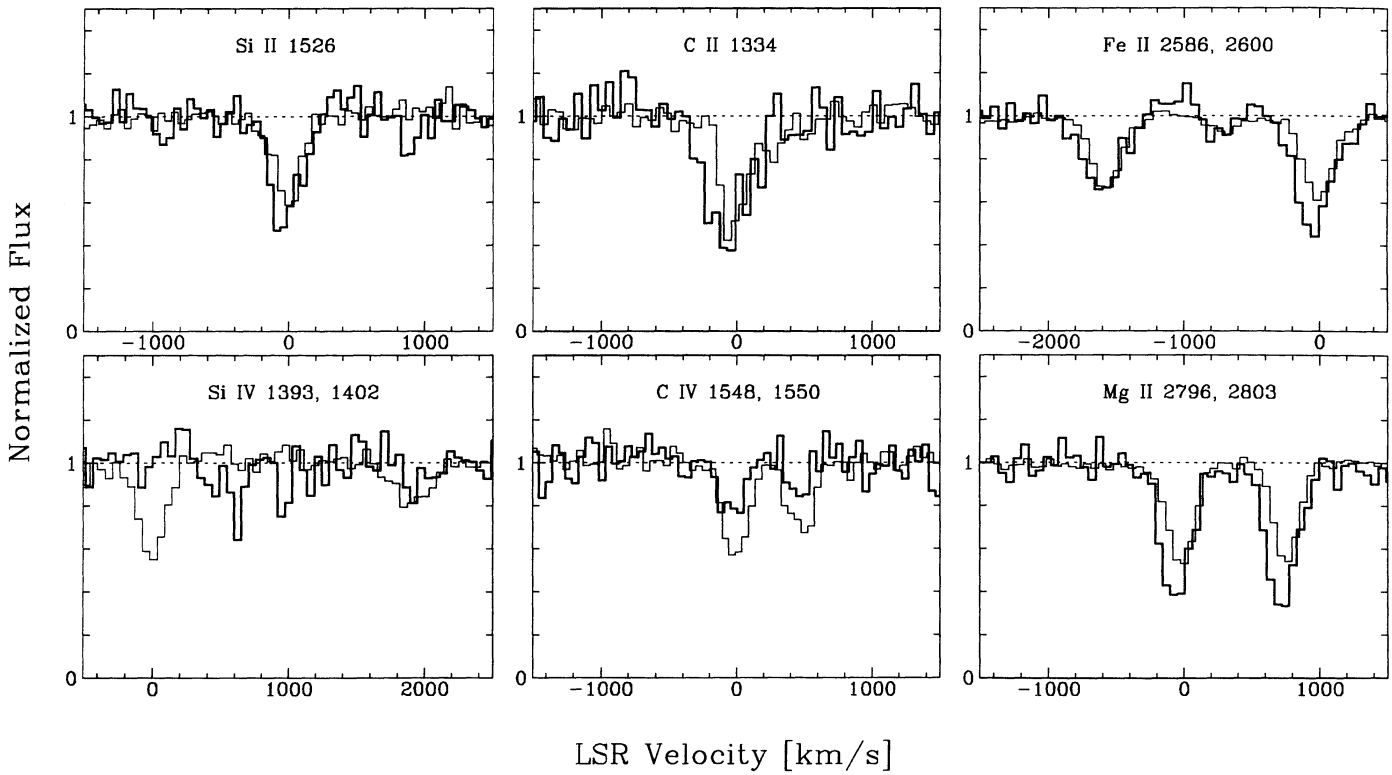

FIG. 6*a*

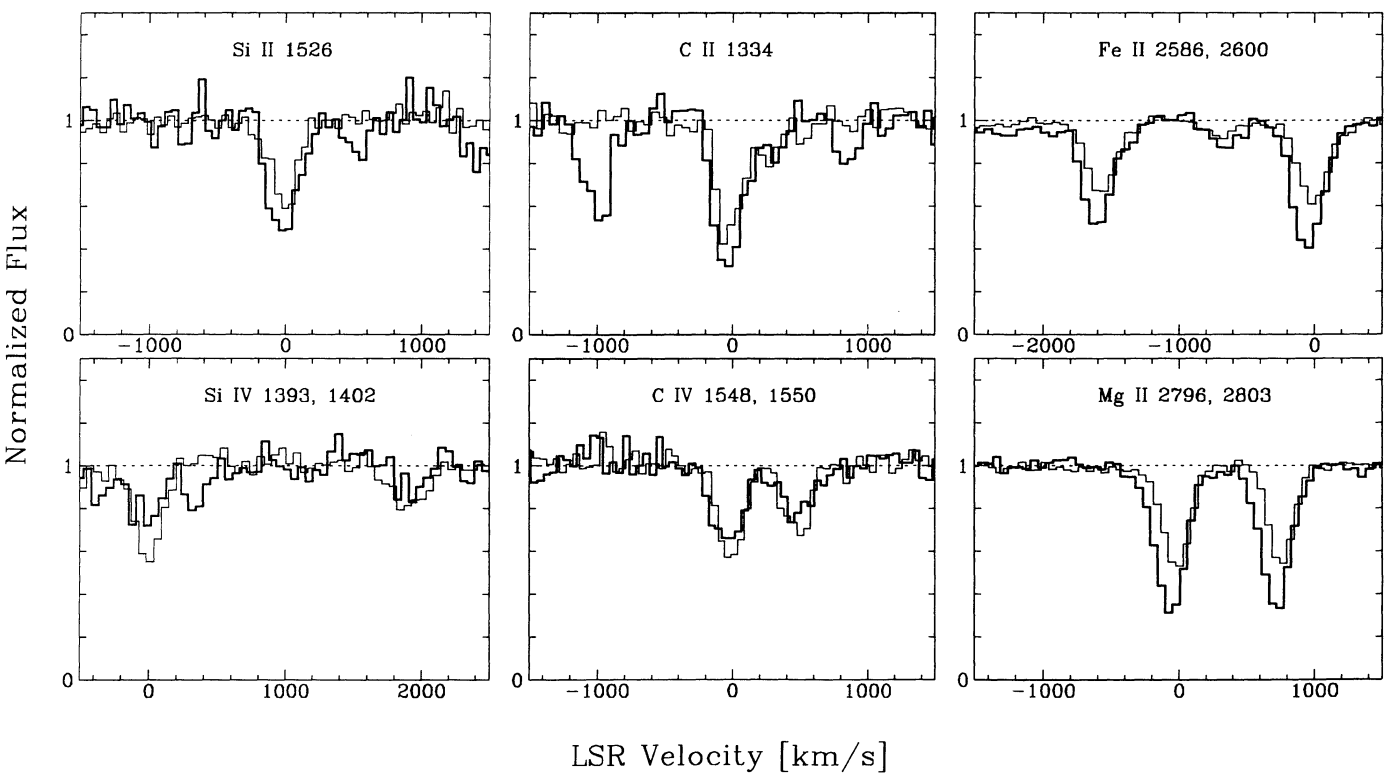

FIG. 6*b*

FIG. 6.—Galactic absorption toward (*a*) PG 1259+593, (*b*) H1821+643, and (*c*) 3C 351 is compared with absorption toward 3C 273. In each case the 3C 273 data are shown with the light line. For each object the various panels illustrate continuum normalized profiles vs. LSR velocity referenced to the following lines: Si II λ1526.71, Si IV λ1393.76, C II λ1334.53, C IV λ1548.20, Fe II λ2600.17, Mg II λ2796.35. Additional absorption features appearing in the various panels (with their apparent velocities in parentheses) are Si IV λ1402.77 (+1939), C II* λ1335.71 (+265), C IV λ1550.77 (+498), Fe II λ2586.65 (−1560), Mn II $\lambda\lambda$2576.88 (−2687), 2594.50 (−654), 2606.17 (+692), and Mg II λ2803.53 (+770).

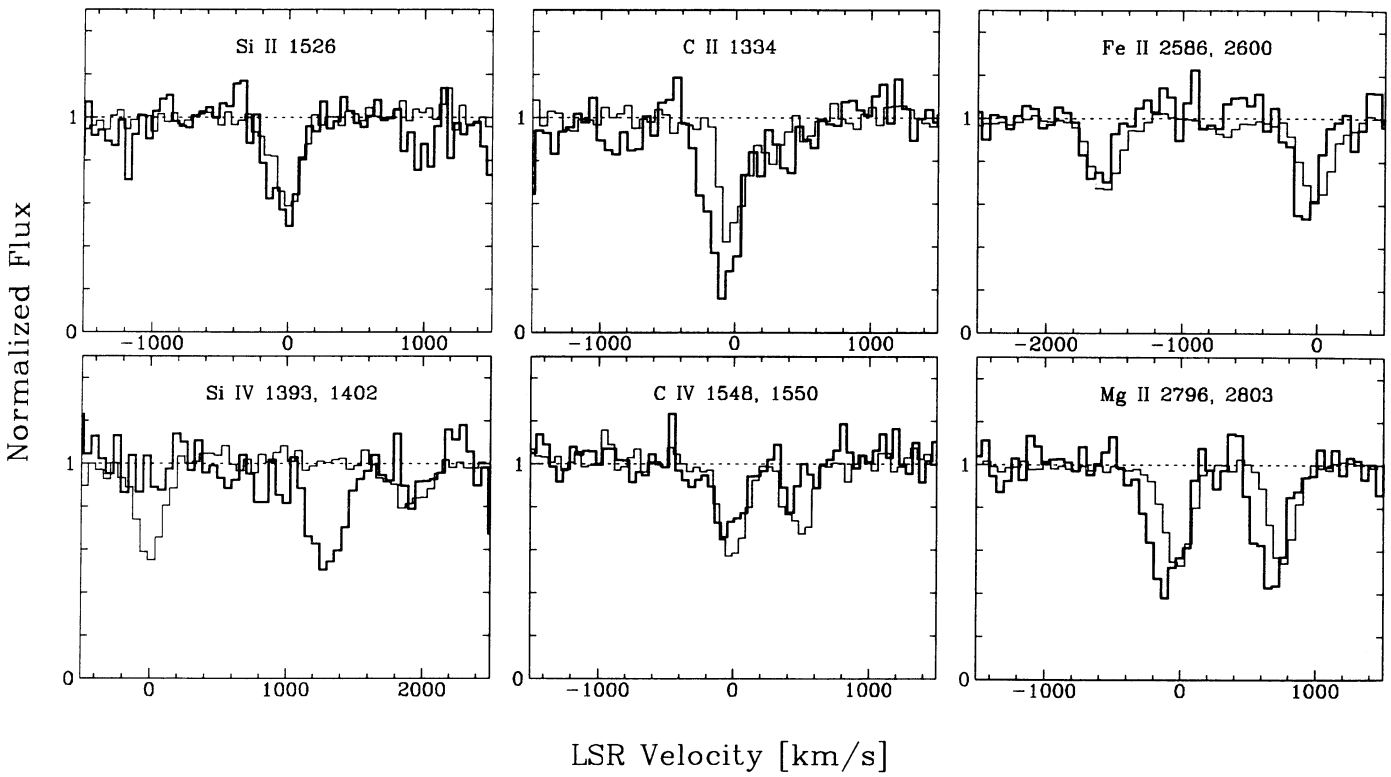

FIG. 6c

shown with light lines. The comparison with the 3C 273 sight line is particularly instructive because of the quality of the 3C 273 data and because the sight line exhibits a relatively simple kinematical structure with relatively symmetric H I emission extending to $v_{LSR}(-) = -62$ km s^{-1} and $v_{LSR}(+) = +46$ km s^{-1} (see Table 1 and Fig. 2). In contrast, for the direction to PG 1259+593, $v_{LSR}(-) = -160$ km s^{-1} and $v_{LSR}(+) = +28$ km s^{-1}. Thus we might expect the ultraviolet absorption-line profiles for the two objects to line up reasonably well on the positive velocity wing and to deviate on the negative velocity wing as is evident in Figure 6a.

From Figure 6*a* we can draw the following conclusions. The strong low-ionization metal lines in the spectrum of PG 1259+593 exhibit significant extensions to large negative velocities. For example, note that the deep portions of the Mg II and C II lines for PG 1259+593 are shifted by approximately -100 km s^{-1} compared with the measurements for 3C 273. We evidently are seeing absorption in the strong metal lines of Mg II, Fe II, C II, and Si II due to gas at large negative velocities associated with Complex *C III*. Absorption by Si IV is not evident in the spectrum of PG 1259+593. However, strong absorption by C IV is present, and the centroid of the absorption is shifted approximately -50 km s^{-1} compared with that seen toward 3C 273. The C IV absorption toward PG 1259+593 may be in part associated with the intermediate-velocity gas due to Complex C *II* seen in the H I emission profile of Figure 2.

The FOS data for PG 1259+593 imply that the gas in the high-velocity structure *C III* contains heavy elements. However, the severity of the blending with absorption by gas at lower velocity makes any quantitative estimate of the abundances in the high-velocity gas quite uncertain. Unfortunately, PG 1259+593 is rather faint for GHRS intermediate-resolution spectroscopy, and alternative brighter sources will be required for higher resolution follow-up spectroscopy designed to obtain reliable abundance estimates.

8. ABSORPTION IN THE OUTER MILKY WAY

There are very strong ultraviolet absorption lines in the spectra of H1821+643 and 3C 351. These two quasars are situated in directions ($l = 94\overset{\circ}{.}0$, $b = 27\overset{\circ}{.}4$ for H1821+643 and $l = 90\overset{\circ}{.}1$, $b = 36\overset{\circ}{.}4$ for 3C 351) which pass through the warp of the outer Milky Way. In these directions the distant H I associated with the warp shows up at velocities between approximately -100 and -200 km s^{-1}. Maps of the distribution of H I in the outer Galaxy are found in Burton & te Lintel Hekkert (1986) and Diplas & Savage (1991). In the longitude range from approximately 70° to 140° the warp of the outer Galaxy has been traced to positive latitudes as large as 25°–35° (Wakker & van Woerden 1991; Diplas & Savage 1991). The H I 21 cm data (LS93a) reveal broad negative velocity emission toward H1821+643 centered at $v_{LSR} = -99$ km s^{-1} and approximately described by a Gaussian profile with FWHM = 72 km s^{-1} and N(H I) = 1.45 × 10^{19} atoms cm^{-2}. Toward 3C 351 weak H I emission extends from -107 to -198 km s^{-1} with N(H I) = 0.90 × 10^{19} atoms cm^{-2}. The high negative velocity emission toward each of these objects is likely associated with the Galactic warp, although in the case of 3C 351 the emission may be associated with high-velocity cloud Complex *C*, which appears to connect with the warped outer arm of the Galaxy (see Wakker & van Woerden 1991 and references therein). It is possible that portions of Complex *C* may have their origins in the warped outer regions of the Galaxy. The gas in the warped outer portions of the Galaxy is

sometimes referred to as the outer arm complex. Habing (1966) and Kepner (1970) showed that gas associated with the outer arm reaches very large heights above the Galactic plane defined by the inner Galaxy.

The very large absorption-line equivalent widths for Galactic gas seen in the spectra of H1821+643 and 3C 351 imply that we are seeing high-velocity absorption in the ultraviolet. The equivalent widths are listed in Table 2, where the values can be compared with those for 3C 273. In Figures 6*b* and 6*c* we compare the absorption-line profiles for the sight line to H1821+643 and 3C 351 to that found toward 3C 273. Note that for the purpose of this comparison $v_{\rm LSR}(-) = -198$ km s^{-1} instead of -86 km s^{-1}, as listed in Table 1, is used for 3C 351 to bring the velocity scale into the LSR system. This is done to take into consideration the presence of weak HVC emission between -198 and -107 km s^{-1} (see § 3 and Table 1). The profile comparisons reveal that the large equivalent widths for H1821+643 and 3C 351 are likely due to extensions of the profiles to large negative velocities. For example, note that for Mg II $\lambda\lambda$2796.35 and 2803.53 the profiles for H1821+643 and 3C 351 align well with those of 3C 273 at positive velocity but the profiles of H1821+643 and 3C 351 have negative extensions approximately -100 km s^{-1} greater than seen toward 3C 273. This large a negative velocity extension implies that Mg II absorption is occurring in the gas associated with the warped outer Galaxy seen in H I 21 cm emission from approximately -100 to -160 km s^{-1} toward each quasar. The measurements imply the existence of Mg II, Fe II, Si II, and C II in the gas of the outer Milky Way. Because of the severe blending of the high-velocity absorption with low-velocity absorption, we will not attempt to establish abundance limits for the gas in the outer Galaxy.

A very interesting comparison in Figure 6*b* concerns the C IV $\lambda\lambda$1548.20 and 1550.77 doublet absorption toward H1821+643. Although the C IV lines are weaker than the strong lines of the singly ionized metals, the C IV absorption appears to behave like the absorption produced by the strong singly ionized metal lines. In particular, the well-observed line λ1548.20 aligns with the 3C 273 profile on the positive velocity side but extends to a larger negative velocity by approximately -70 to -100 km s^{-1}. In Figure 6*c* it is apparent that C IV λ1548.20 toward 3C 351 is shifted approximately -50 to -80 km s^{-1} compared with the 3C 273 measurement. With such a modest velocity shift the accuracy of our velocity zero-point correction may be called into question. We therefore display in Figure 7*a* comparisons between the profiles of Si II λ1526.71 and C IV λ1548.20 for PG 1259+593 (see § 7), 3C 351, H1821+643, and 3C 273. In Figure 7*b* we compare absorption by Mg I λ2852.96 and Mg II λ2796.35. By interconparing the data obtained with the same grating (G130H for Fig. 7*a* and G270H for Fig. 7*b*), we eliminate any possible systematic velocity offset between the spectra of two different gratings. The small wavelength difference between the Si II and C IV lines or between the Mg I and Mg II lines also minimizes the effects of wavelength or velocity uncertainties associated with errors in the FOS dispersion constants. It is significant that the C IV λ1548.20 profiles for 3C 351 and H1821+643 show velocity extents similar to those of Si II λ1526.71. The Mg I and Mg II comparison in Figure 7*b* reveals that the small wavelength adjustments we have adopted for these objects are likely correct. Note that the weaker Mg I lines which mostly trace the denser gas of the Galactic disk have their region of maximum absorption approximately centered on $v = 0$ km s^{-1} for 3C 351, H1821+643, and 3C 273, as expected based on the 21 cm data toward these objects. In contrast, the extremely strong Mg II absorption grows to negative velocity for 3C 351 and H1821+643, but grows symmetrically to negative and positive velocity for 3C 273.

The good profile correspondence between the C IV λ1548.20 and the Si II λ1526.71 absorption for 3C 351 and H1821+643 in Figure 7*a* implies that the Si II and C IV absorption occur over a roughly similar range of velocities. Since the strong low-ionization absorption recorded in the lines of Mg II, Fe II, Si II, and C II is clearly connected with the high-velocity gas of the outer Galaxy, it seems safe to conclude that the C IV absorption is also in part associated with that gas.

If confirmed through higher resolution measurements, the negative velocity extensions seen in the C IV lines toward H1821+643 and 3C 351 would imply that C IV absorption is occurring in the outer Milky Way at Galactocentric distances exceeding roughly 20 kpc. This crude distance estimate follows from the study of H I in the outer Galaxy by Diplas & Savage (1991). Toward H1821+643 and possibly even toward 3C 351, the high negative-velocity gas appears to be associated with the warped outer region of the Milky Way. The warped gas in these directions appears to extend to well beyond Galactocentric distances of 20 kpc and to have midplane heights z exceeding $\sim +3$ kpc, and to have a thickness of up to ~ 10 kpc (see Figs. 4*a* and 4*b* in Diplas & Savage 1991).

The origin of the ionization of the C IV at such large distances from the center of the Galaxy is of interest because it is not obvious that a substantial Galactic fountain would occur in that region of the Galaxy. Perhaps at large Galactocentric distances the production of C IV is from the extragalactic EUV background radiation. The very existence of mixed ionization absorption at large Galactocentric distances is important; it lends support to the idea that some quasar absorption lines, including those of mixed ionization, may be produced in the outer regions or halos of normal galaxies (Bahcall & Spitzer 1969).

9. THE GALACTIC SCALE HEIGHT OF C IV

The four quasars observed in the far-UV with the FOS G130H grating (3C 273, PG 1259+593, H1821+643, and 3C 351) show strong absorption in the lines C IV $\lambda\lambda$1548.20 and 1550.77. The measured equivalent widths and estimates of the inferred C IV column density based on a simple one-component Doppler-broadened curve of growth are listed in Table 5. Those results are supplemented with measurements for PKS 0405−12 from Bahcall et al. (1993b). Extensive measurements with the *IUE* satellite have revealed that Milky Way halo C IV absorption lines of the strength found in these objects are often only modestly saturated, since the value of the Doppler spread parameter, b, characterizing the high-ionization line absorption is typically 25–50 km s^{-1} (Sembach & Savage 1992). Therefore, the use of the simple curve of growth to obtain estimates of N(C IV) is probably valid even though the procedure would be unreliable if applied to the very strongly saturated singly ionized metal lines. The measurements for PKS 0405−12 appears to be an exception, in that the two equivalent widths reported imply a high degree of line saturation. The value of N(C IV) reported for this object is a lower limit.

Measures of N(C IV) through the entire halo to extragalactic objects are important for improving the current estimates of the Galactic scale height of this important ion. In Figure 8 we

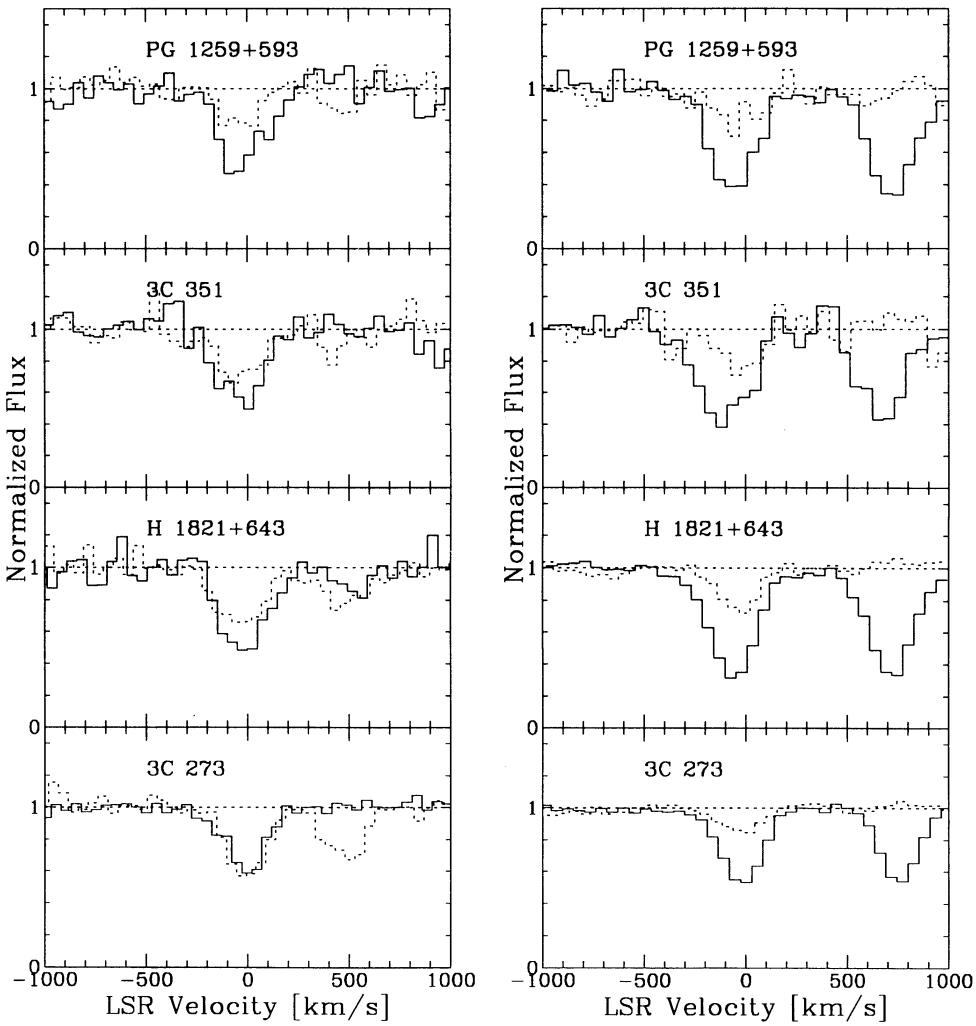

FIG. 7a

FIG. 7b

FIG. 7.—(*a*) Comparison of Galactic absorption toward PG 1259+593, H1821+643, 3C 351, and 3C 273 in the lines of Si II λ1526.71 (*solid line*) and C IV λ1548.20 (*dashed line*). (*b*) The lines of Mg II λ2796.35 (*solid line*) and Mg I λ2852.96 (*dashed line*) are compared. Continuum normalized intensity is plotted against LSR velocity. The λ1550.77 component of the C IV doublet appears at an apparent velocity of 498 km s^{-1}. The Si II data for H1821+643 reveal an additional feature near +500 km s^{-1} attributed to intergalactic Lyα (see Paper I). The Mg II λ2803.53 component of the doublet appears at an apparent velocity of 770 km s^{-1}. Since these comparisons relate measurements obtained with the same grating, of species situated close in wavelength, the errors in the velocity adjustment procedures should be minimized.

show values of the logarithm of the column density of C IV perpendicular to the Galactic plane, log N(C IV) $|\sin b|$, plotted against the logarithm of distance away from the plane, log $|z\,(\mathrm{kpc})|$. The data plotted with log $|z\,(\mathrm{kpc})| < 2$ are from the *IUE* measurements analyzed by Sembach & Savage (1992) for Milky Way stars and for stars in the LMC and SMC. The measurements plotted at log $|z\,(\mathrm{kpc})| \sim 3$ are for the five quasars listed in Table 5. In the case of 3C 273 we have chosen to use the result from Savage et al. (1993) based on GHRS intermediate-resolution observations (see footnote *b* to Table 5).

To estimate the C IV exponential scale height from the data shown in Figure 8, we adopt the procedure of Savage, Edgar, & Diplas (1990), which assumes that the distribution in C IV away from the plane is described by an exponential layer that is intrinsically patchy, so that any measurement will deviate from the mean by a factor which has a dispersion 10^{σ_p}. The logarithmic uncertainty associated with each measurement is then assumed to have two components which add in quadrature: one is from the observational error, σ_o, and the other from the patchy distribution of the ISM, σ_p. The model parameters, including the exponential scale height h and the midplane density n_0(C IV), are determined from minimizing the χ^2 of the fit of the model to the data. The value of σ_p is adjusted during the fit such that the minimal reduced χ^2 is unity. In working with the inhomogeneous data set from Sembach & Savage (1992), we have adopted their errors for the high-quality measurements for the 12 stars listed in their Table 8. However, for the objects from literature listed in their Table 7 we adopt a logarithmic observing error, $\sigma_o = 0.15$. This error is about 2–3 times larger than the ones derived by Sembach & Savage (1992) based on multiple *IUE* observations.

The best-fit result shown as the heavy solid curve in Figure 8 was obtained for an intrinsic scatter $\sigma_p = 0.31$ dex ($10^{\sigma_p} = 2.04$), which implies that the C IV distribution is indeed quite irregular. The best-fit exponential scale height and midplane

TABLE 5

C IV EQUIVALENT WIDTHS AND COLUMN DENSITIES

QSO	$W_\lambda(1548) \pm \sigma$ (Å)	$W_\lambda(1550) \pm \sigma$ (Å)	log N(C IV)[a] $\pm \sigma$ (atoms cm^{-2})
3C 273	0.54 ± 0.01	0.39 ± 0.02	14.50[b] ± 0.08
PG 1259+593	0.28 ± 0.02	0.14[c] ± 0.02	13.84 ± 0.10
H1821+543	0.53 ± 0.03	0.36 ± 0.03	14.41 ± 0.11
3C 351	0.45 ± 0.04	...	>14.04 ± 0.15
PKS 0405−12	0.35[d] ± 0.08	0.36[d] ± 0.12	>13.93 ± 0.15

[a] Values of log N(C IV) are based on the doublet method. For 3C 351 and PKS 0405−12 the values of the column density which are indicated as a lower limit are from the equivalent width for the 1548 Å line and assume no line saturation.

[b] The Key Project FOS result for 3C 273 is listed here. The C IV column density, from the GHRS observations of Savage et al. 1993, is log N(V IV) = 14.61 ± 0.05. The GHRS result is plotted in Figs. 8 and 9.

[c] Measurements for $W_\lambda(1550)$ for PG 1259+593 are from the incomplete sample of Key Project absorption-line measurements.

[d] The C IV equivalent widths for PKS 0405−12 listed here are from Bahcall et al. 1993b. PKS 0405−12 is in the Galactic direction $l = 204.°93$, $b = -41.°76$.

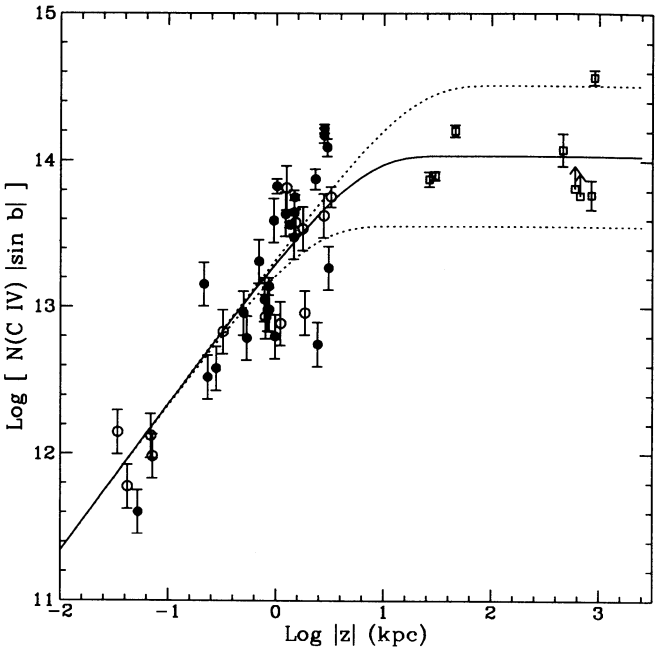

FIG. 8.—Plot of log N(C IV) |sin b| vs. log |z(kpc)|. Circles are for sight lines to Galactic stars, and squares are for extragalactic sight lines. Measurements plotted with log |z(kpc)| < 2 are from the *IUE* data listed in Tables 7 and 8 of Sembach & Savage (1992) and include *IUE* measurements to Galactic stars and stars in the LMC and SMC. The measurements plotted near log |z| ~ 3 are for the five quasars listed in Table 5. In the case of 3C 273 we have plotted the result based on the GHRS measurements of Savage et al. (1993). The measurements for objects situated within 50° of the direction of the Galactic center are plotted with filled symbols. The solid line shows the result of a χ^2 fit to the data for a plane-parallel Galactic atmosphere with an assumed exponential density stratification. The χ^2 fitting process we employ allows for the inhomogeneous distribution of C IV. The best fit is for an exponential scale height h = 4.9 kpc and midplane density n_0(C IV) = 0.71 × 10^{-8} atoms cm^{-3} The dashed lines show curves for C IV exponential scale heights 3 times larger and smaller than the best-fit value.

density are $h = 4.9^{+1.8}_{-1.3}$ kpc and n_0(C IV) = 0.71 × 10^{-8} atoms cm^{-3}. The dashed lines in Figure 8 illustrate simple exponential distributions for the best-fit midplane density, but scale heights 3 times larger and 3 times smaller than the best-fit value. Since two of the reported C IV column densities in Table 5 are lower limits, the true C IV scale height might be somewhat larger than that derived here.

Measurements for objects within 50° of the direction of the Galactic center are plotted with the filled symbols in Figure 8. There is no apparent difference between measurements plotted with filled or open symbols which indicates that the C IV distribution in the inner Galaxy roughly corresponds to that in the solar vicinity (see Sembach & Savage 1992). Unfortunately, none of the extragalactic objects (denoted by squares) lie in the direction of the inner Galaxy.

There is no theoretical basis for fitting the C IV data with a simple exponential panel-parallel scale-height model as was done in Figure 8. Given the irregular distribution of C IV that we observe, alternative plane-parallel model distributions and even spherical halo models may provide equally acceptable fits to the data. To illustrate the latter case, we fit the C IV data to a spherical halo model in which the gas density falls off exponentially with radial distance r from the Galactic center,

$$n(r) = n_0(\text{C IV}) \exp(-r/R),$$

where n_0(C IV) is the volume density of the C IV gas at the Galactic center and R is the exponential scale length. For given values of n_0(C IV) and R, one can estimate the integrated C IV column density along any given sight line from the position of the Sun to an observed object, and compare the expected column density from the model with the observed column density. The model fit assumes the Sun is 8.5 kpc from the center of the Galaxy. The best-fit values of n_0(C IV) and R are then determined from minimizing the χ^2 of the comparison. Similar to the plane-parallel model, the logarithmic uncertainty associated with each measured C IV column density is assumed to be the quadratic sum of the observational error σ_o and an error σ_p that is due to the intrinsic patchiness of the C IV gas distribution. The best-fit spherical halo model is obtained for R = 6.9 kpc, n_0(C IV) = 1.74 × 10^{-8} atoms cm^{-3}, and σ_p = 0.30 dex (10^{σ_p} = 2.00). The fact that the patchiness parameter σ_p for the spherical halo model is about the same as for the plane-parallel model shows that the data do not set strong constraints on which model best describes the C IV distribution. This is illustrated in Figure 9, where we show plots of the observed values of log N(C IV) compared with the predicted values for the plane-parallel model (in Fig. 9*a*) and for the spherical model (in Fig. 9*b*). The data are coded the same as in Figure 8, with the extragalactic data points plotted as squares. Given the patchiness in the distribution of the C IV, we cannot determine which model provides the best fit with the current set of C IV data.

We have not tried to perform a similar scale-height analysis for Si IV, which produces absorption lines substantially weaker than C IV. Generally the Si IV absorption is below the FOS detection threshold. Note that Si IV λ1393.76 seems anomalously strong toward 3C 273 because it is contaminated by intergalactic Lyα absorption (see Savage et al. 1993).

The exponential C IV scale height for the plane-parallel model derived here compares favorably with the value 4.7 kpc obtained recently by Sembach & Savage (1992). Theories concerning the origin of C IV at such large distances from the Galactic plane are discussed in their paper. A proper theory will need to explain the large extension away from the plane and also the patchiness of the gas, which causes the large spread in Figures 8 and 9.

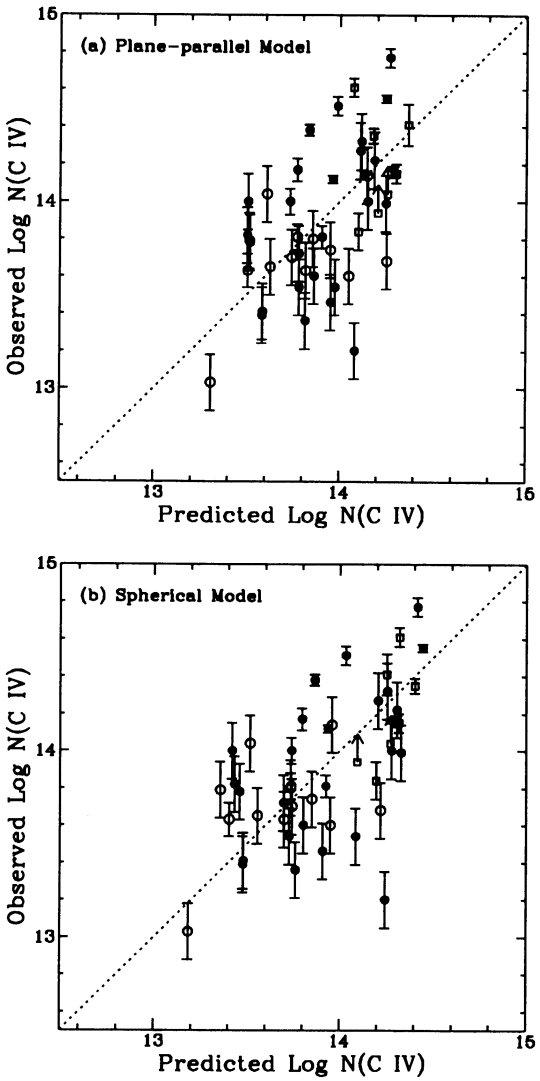

FIG. 9.—Observed and predicted logarithmic column densities for C IV are compared (*a*) for the best-fit plane-parallel Galactic halo model and (*b*) for the best-fit spherical halo model. The best-fit plane-parallel model has an exponential scale height of 4.9 kpc, a C IV midplane density of 0.71×10^{-8} atoms cm^{-3}, and a patchiness parameter of $\sigma_p = 0.31$ dex. The best-fit spherical halo model has a Galactocentric exponential scale length of 6.9 kpc, a Galactocentric C IV density of 1.74×10^{-8} atoms cm^{-3}, and a patchiness parameter of $\sigma_p = 0.30$ dex. The symbol coding in Fig. 9 is the same as in Fig. 8.

10. MILKY WAY ABSORPTION VERSUS ABSORPTION IN QUASAR METAL-LINE SYSTEMS

The narrow metal absorption lines seen in spectra of high-redshift QSOs are generally believed to arise from gaseous material in high-redshift galaxies (Bahcall & Spitzer 1969; Bergeron & Boisse 1991; Yanny & York 1992). In particular, the damped Lyα systems, a subset of the metal-line absorption systems, are believed to arise when the QSO sight lines intersect the disks or the protodisks of spiral galaxies at high redshifts (Wolfe et al. 1986; Wolfe 1988). Our understanding of the damped Lyα systems will be greatly enhanced by comparing their absorption properties with those due to local disk galaxies.

While sight lines through the disks of nearby external galaxies toward bright background sources are rare, UV absorption arising from the disk and halo gas of the Milky Way has been observed with the *IUE* against bright halo stars (Savage & Massa 1987; Danly 1989; Sembach & Savage 1992) and stars in the Large and Small Magellanic Clouds (Savage & de Boer 1981; Fitzpatrick & Savage 1983). Reliable high-resolution observations of Milky Way absorption against other extragalactic sources (active galactic nuclei [AGNs] and QSOs) were generally not possible with the *IUE*, owing to the faintness of even the brightest AGNs and QSOs. Savage et al. (1993) have compared the *mean* absorption-line strengths of over a dozen commonly detected low- and high-ionization lines for a sample of damped Lyα systems with the Milky Way disk and halo absorption lines toward the QSO 3C 273 obtained with the *HST*, and found the absorption-line strengths to be similar.

In this section we extend the discussion of Savage et al. (1993), taking advantage of data toward the three new sight lines, namely, H1821+643, 3C 351, and PG 1259+593, for which G130H observations have been obtained. These data are supplemented with the high-quality *IUE* observations toward the star HD 5980 in the SMC (Fitzpatrick & Savage 1983) and the star HD 36402 in the LMC (Savage & de Boer 1981; Sembach & Savage 1992). Observations toward Milky Way halo stars are excluded in order not to bias the results with their relatively short path length ($|z| < 2$ kpc) through the Milky Way halo.

The comparison is illustrated in Figure 10, in which we plot the distribution of absorption-line strengths of individual systems (sight lines) in kilometers per second (cW_λ/λ) for the commonly detected low- and high-ionization species. The vertical lines are for the damped Lyα systems, while the circles are for the Milky Way sight lines. Dashed lines and circles represent upper limits on the equivalent widths. The sample of damped Lyα systems is from the compilation of Lu (1991). There is a total of 33 damped systems included, but not every line is observed for every system. The mean H I column density of the damped sample is 1.1×10^{21} atoms cm^{-2} at a mean redshift of 2.4. In comparison, the mean H I column density of

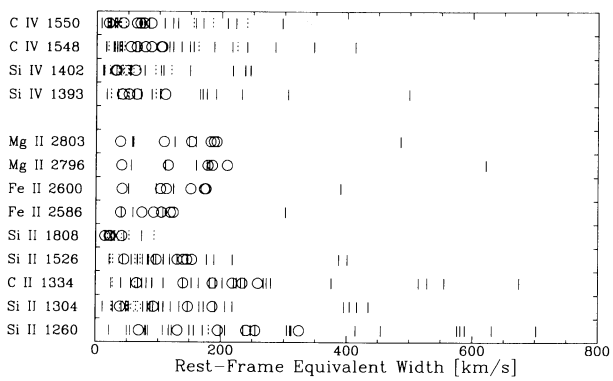

FIG. 10.—Comparison of Galactic and extragalactic absorption-line rest-frame equivalent widths for the commonly detected low- and high-ionization lines seen in quasar damped Lyα absorption-line systems. The vertical lines are for damped Lyα systems at a mean redshift of 2.4, while the circles are for Milky Way sight lines. Dashed lines or circles denote upper limits to the equivalent widths. The equivalent widths, $W_v = W_\lambda c/\lambda$, are expressed in the physically meaningful units of velocity, km s^{-1}. Since most of the low-ionization lines illustrated are generally strongly saturated, the equivalent width is a measure of the kinematical complexity of the absorption and is not a good measure of column density. A number of biases influence the comparison as discussed in the text.

the six Milky Way sight lines is 3.0×10^{20} atoms cm^{-2} for a half-disk.

A casual glance at Figure 10 gives the impression that the Milky Way sight lines and the damped Lyα systems are different in that the absorption from damped Lyα systems is generally stronger. However, there are several selection biases that affect the comparison. First, while the Milky Way sight lines sample the disk and halo gas of the Milky Way alone, the damped Lyα systems may not represent a homogeneous set of absorbers. Specifically, a small fraction of the damped systems may actually arise from galaxies residing in clusters of galaxies, in which case the sight line will also sample the intracluster gas and halo gas of other cluster members. Second, the Si II λ1260, Si II λ1304, and C II λ1334 lines, which are the very low ionization lines that show a particularly large difference in the two distributions, are also the ones closest to the Lyα line in wavelength, and are therefore often affected by blending with Lyα forest absorption. A third bias is due to the fact that the Milky Way absorption used in the comparison is through only half of the Milky Way disk and halo, while the damped Lyα sight lines presumably sample the entire disk and halo of high-z galaxies. All of these selection biases will tend to make the Milky Way absorption relatively weaker.

It is interesting to see for the low-ionization lines that the Milky Way absorption actually tracks the *bulk* of damped Lyα systems. However, the differences in the distributions of high-ionization lines (Si IV and C IV) between the Milky Way gas and damped Lyα systems are substantial. The high-ionization lines mostly occur at wavelengths longward of Lyα emission, so blending with Lyα forest absorption should not be a problem. However, the high-ionization lines are more easily affected by the third selection bias discussed above. Most low-ionization absorption lines in the case of Milky Way gas are produced in the cold and warm disk gas; the lines are strong and saturated. Therefore, the low-ionization line strengths are dominated by the kinematic behavior of the gas in the disk and low halo. In contrast, the high-ionization lines are dominated by halo gas, and the lines are generally only moderately saturated (cf. Savage et al. 1993). Thus doubling the path lengths (i.e., correcting for the third selection bias) of the Milky Way sight lines is likely to increase the high-ionization line strength owing to the approximate doubling of the column density of the highly ionized halo gas, while leaving the strongly saturated low-ionization lines relatively unaffected unless the doubling of the path increases the kinematical extent of the absorption.

The data in Figure 10 indicate that many damped Lyα absorption-line systems have mixed-ionization absorption-line strengths roughly similar to that found toward the Milky Way sight lines included in our study. Those systems that are most similar have velocity equivalent widths for the strong low-ionization metal lines ranging from $\sim$50 to $\sim$250 km s^{-1}. Among the damped Lyα systems plotted, such systems represent an appreciable fraction ($\sim$60%–80%). We emphasize that the similarity implies a similarity in the kinematical behavior of the different absorption media and not necessarily in elemental abundances. The current sample of Milky Way absorption (consisting of six sight lines with full UV spectral coverage) is still very small. Future *HST* Key Project data will permit a better comparison to be made.

11. SUMMARY

The results of our study of the zero-redshift Galactic absorption lines found in the spectra of 15 quasars observed with FOS at a resolution of $\sim$230 km s^{-1} are as follows:

1. As noted in Paper I, Milky Way absorption lines comprise approximately 44% of all absorption lines seen in the first group of Key Project FOS spectra.
2. The interpretation of the Milky Way data is aided by having access to independent high-quality measurements of H I 21 cm emission toward all the quasars (LS93a). The H I data are used to make small adjustments to the FOS wavelength scale to bring the UV data onto an LSR velocity system.
3. Milky Way lines observed in the highest quality data for 3C 273 and H1821+643 include lines from H I, C II, C II*, C IV, N I, O I, Mg I, Mg II, Al II, Al III, Si II, Si III, Si IV, S II, Mn II, Fe II, and Zn II.
4. The strong singly ionized metal lines of Fe II $\lambda\lambda$2382.77, 2586.65, and 2600.17 and Mg II $\lambda\lambda$2796.35 and 2803.53, recorded in most of the spectra, permit a sensitive search for metal-line analogs to the high-velocity clouds seen in H I 21 cm emission.
5. Toward three quasars we detect resolved very high velocity ($v < -250$ km s^{-1}) Mg II line absorption. Toward four quasars we detect blended high-velocity absorption (-250 km s$^{-1} < v < -100$ km s^{-1}). Therefore, seven of the 15 quasars observed in this limited sample show high-velocity or very high velocity metal-line absorption detectable with FOS with $\lambda/\Delta\lambda \sim 1300$.
6. Limits to the Mg-to-H abundance ratio obtained for the three detections of very high velocity Mg II absorption imply gas-phase Mg abundances for the very high velocity gas ranging from more than 0.059 to more than 0.32 times the solar abundance. These limits may be affected by differences in the sampling geometry between the metal-line data (infinitesimal solid angle) and the H I 21 cm measurements (21′ beam).
7. The sight line to PG 1259+593 reveals absorption in the lines of Mg II, Fe II, C II, and Si II which is due in part to absorption in high-velocity cloud Complex *C III*.
8. The sight lines (H1821+643 and 3C 351) which extend through the warped outer Galaxy exhibit strong absorption from singly ionized metals and highly ionized gas (i.e., C IV) at velocities corresponding to absorption in the outer Galaxy.
9. In all cases where high-velocity H I emission is seen, we see corresponding high-velocity metal-line absorption.
10. The measurements for C IV absorption to extragalactic objects are important for estimating the Galactic scale height of C IV. Combining the results for the sight lines to 3C 273, H1821+643, PG 1259+593, and 3C 351 with results in the literature we derive a Galactic C IV scale height of $4.9^{+1.8}_{-1.3}$ kpc and a C IV midplane density of 0.71×10^{-8} atoms cm^{-3}. The C IV distribution is quite inhomogeneous. Alternative C IV model distributions including, for example, a spherical halo with a Galactocentric exponential scale length of 6.9 kpc provide equally acceptable fits to the C IV data.
11. An appreciable fraction of damped Lyα absorption-line systems at $z \sim 2.4$ observed from the ground have mixed-ionization absorption-line characteristics roughly similar to that seen toward six sight lines through the Milky Way disk and halo for which data extend to 1150 Å. This implies a similarity in the kinematic properties of the different absorbers but not necessarily a similarity in elemental abundances.

We appreciate the assistance of the FOS team in providing an excellent instrument and the calibration software used in the basic processing of the Quasar Absorption Line Key

Project spectra. We thank R. Lucas and the User Support Branch of the Space Telescope Science Institute for their assistance with the preparation and execution of the observations reported here. This work was supported in part by NASA grant GO-2424.01 from the Space Telescope Science Institute, which is operated by the Association of Universities for Research in Astronomy, Inc., under NASA contract NAS 5-26555. F. J. L. acknowledges support from the National Radio Astronomy Observatory, which is operated by Associated Universities, Inc., under a cooperative agreement with the National Science Foundation.

REFERENCES

Anders, E., & Grevesse, N. 1989, Geochim. Cosmochim. Acta, 53, 197
Bahcall, J. N., et al. 1993a, ApJS, 87, ApJS, 87, 1 (Paper I)
Bahcall, J. N., Jannuzi, B. T., Schneider, D. P., & Hartig, G. F. 1993b, ApJ, 405, 491
Bahcall, J. N., Jannuzi, B. T., Schneider, D. P., Hartig, G. F., Bohlin, R., & Junkkarinen, V. 1991, ApJ, 377, L5
Bahcall, J. N., Jannuzi, B. T., Schneider, D. P., Hartig, G. F., & Green, R. F. 1992, ApJ, 397, 68
Bahcall, J. N., & Spitzer, L. 1969, ApJ, 156, L63
Bajaja, E., Cappa de Nicolau, C. E., Cersosimo, J. C., Loiseau, N., Martin, M. C., Morras, R., Olano, C. A., & Poppel, W. G. L. 1985, ApJS, 58, 143
Bergeron, J., & Boisse, P. 1991, A&A, 243, 344
Bohlin, R. C., Savage, B. D., & Drake, J. 1978, ApJ, 224, 132
Burton, W. B., & te Lintel Hekkert, P. 1986, A&AS, 65, 427
Cardelli, J. A., Clayton, G. C., & Mathis, J. S. 1989, ApJ, 345, 245
Danly, L. 1989, ApJ, 342, 785
Danly, L., Lockman, F. S., Meade, M. R., & Savage, B. D. 1992, ApJS, 81, 125
Dickey, J. M., Crovisier, J., & Kazes, I. 1981, A&AS, 98, 271
Dickey, J. M., & Lockman, F. J. 1990, ARA&A, 28, 215
Diplas, A., & Savage, B. D. 1991, ApJ, 377, 126
Fitzpatrick, E. L., & Savage, B. D. 1983, ApJ, 267, 93
Habing, H. J. 1966, Bull. Astr. Inst. Netherlands, 18, 323
Hulsbosch, A. N. M. 1968, Bull. Astr. Inst. Netherlands, 20, 33
Hulsbosch, A. N. M., & Raimond, E. 1966, Bull. Astr. Inst. Netherlands, 18, 413
Hulsbosch, A. N. M., & Wakker, B. P. 1988, A&AS, 75, 191
Jenkins, E. B. 1989, in Interstellar Processes, ed. D. J. Hollenbach & H. A. Thronson, Jr. (Dordrecht: Reidel), 533
Jenkins, E. B., Savage, B. D., & Spitzer, L. 1986, ApJ, 301, 355
Kepner, M. E. 1970, A&A, 5, 444
Kinney, A. L. 1992, Faint Object Spectrograph Handbook Version 2.0 (Baltimore: STScI)
Liszt, H. S., & Burton, W. B. 1979, ApJ, 228, 105
Lockman, F. J., & Savage, B. D. 1993a, in preparation (LS93a)
———. 1993b, in preparation (LS93b)
Lu, L. 1991, Ph.D. thesis, Univ. Pittsburgh
Morris, S. L., Weymann, R. J., Savage, B. D., & Gilliland, R. L. 1991, ApJ, 377, L21
Morton, D. C. 1991, ApJS, 77, 119
Savage, B. D. 1988, in QSO Absorption Lines, ed. J. C. Blades, D. Turnshek, & C. A. Norman (Cambridge: Cambridge Univ. Press), 195
Savage, B. D., & de Boer, K. S. 1981, ApJ, 243, 460
Savage, B. D., Edgar, R., & Diplas, A. 1990, ApJ, 361, 107
Savage, B. D., Lu, L., Weymann, R. J., Morris, S. L., & Gilliland, R. L. 1993, ApJ, 404, 124
Savage, B. D., & Massa, D. 1987, ApJ, 314, 380
Savage, B. D., & Mathis, J. S. 1979, ARA&A, 17, 73
Schneider, D. P., et al. 1993, ApJS, 87, 45 (Paper II)
Sembach, K. S., & Savage, B. D. 1992, ApJS, 83, 147
Spitzer, L. 1978, Physical Processes in the Interstellar Medium (New York: Wiley)
Turner, B. E. 1988, in Galactic and Extragalactic Radio Astronomy, ed. G. L. Verschuur & K. I. Kellermann (2d ed.; Berling: Springer-Verlag), 154
Wakker, B. P. 1991, A&A, 250, 499
Wakker, B. P., & Schwarz, U. J. 1991, A&A, 250, 484
Wakker, B. P., & van Woerden, H. 1991, A&A, 250, 509
Wolfe, A. M. 1988, in QSO Absorption Lines: Probing the Universe, ed. J. C. Blades, D. A. Turnshek, & C. A. Norman (Cambridge: Cambridge Univ. Press), 297
Wolfe, A. M., Turnshek, D. A., Smith, H. E., & Cohen, R. D. 1986, ApJS, 61, 249
Yanny, B., & York, D. G. 1992, ApJ, 391, 569